SAND2019-13050C

Adaptive Imaging using a Cylindrical, Time-Encoded Imaging System

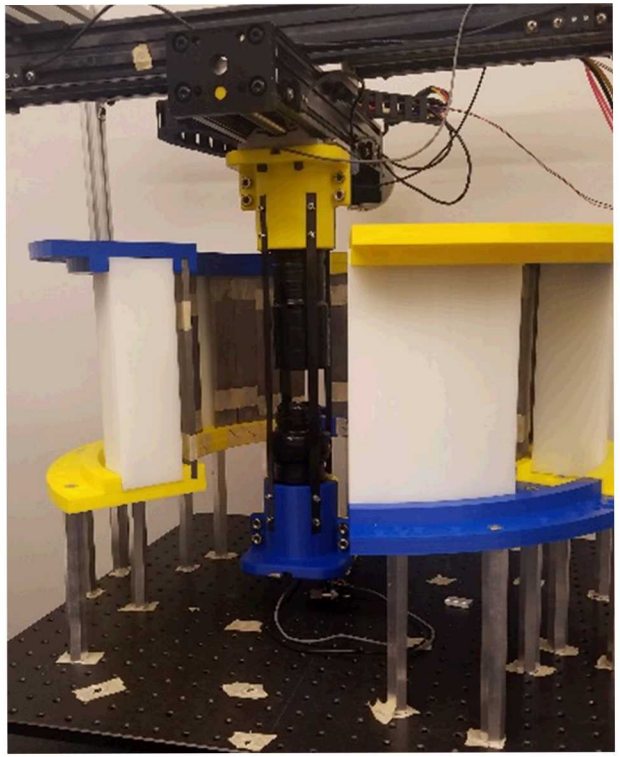

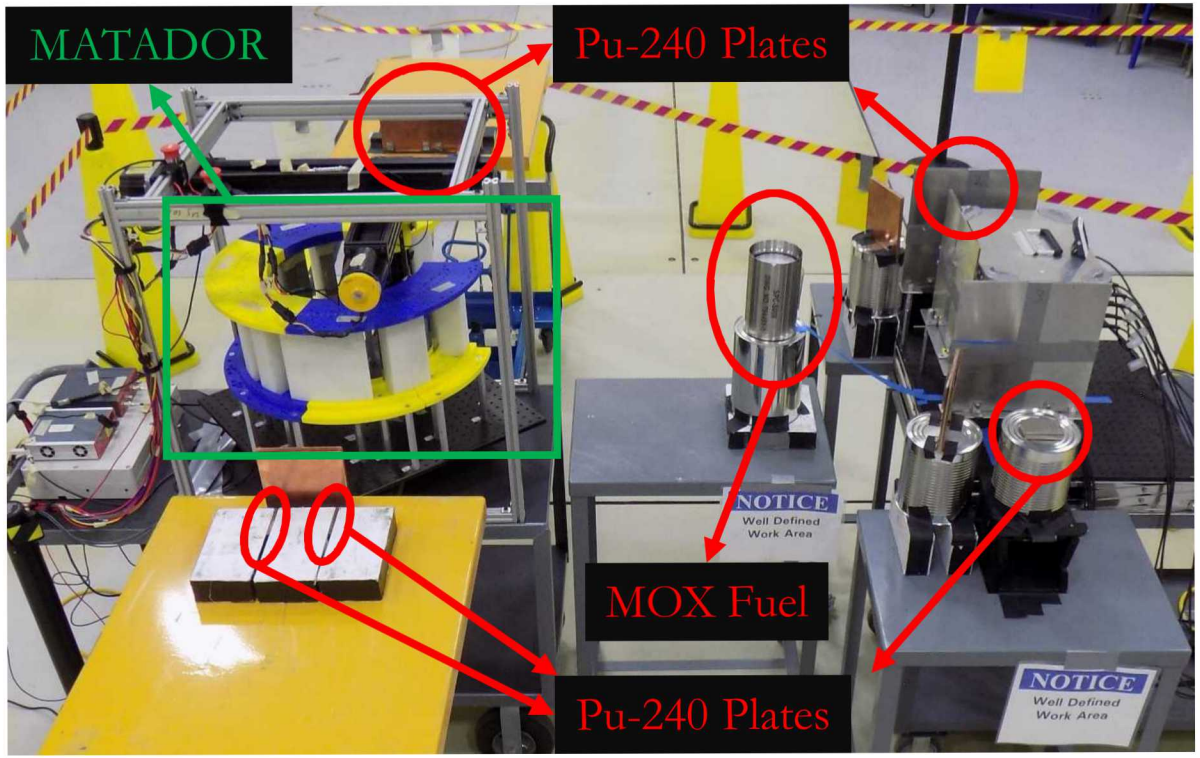

Niral Shah, John Kuchta, Peter Marleau[1] , David Chichester[2], and David Wehe

[1]Sandia National Labs

[2]Idaho National Labs

October 29th, 2019

Sandia National Laboratories is a multimission laboratory managed and operated by National Technology & Engineering Solutions of Sandia, LLC, a wholly owned subsidiary of Honeywell International Inc., for the U.S. Department of Energy's National Nuclear Security Administration under contract DE-NA0003525.

Motivation

Nuclear Non-proliferation and International Safeguards

- Continuous surveillance and accounting of sources within a storage vault or vessel
- Search for undeclared sources in an access restricted setting

Monzano Alarm and Nuclear Material Consolidation Project

Treaty and Disarmament Verification

- Counting warheads instead of delivery vehicles (upgrading New Start)
- Verify Russian ICBMs are not MIRVs
- Verify SNM is separated from high explosives

Google Maps. (2018). 32.1502366, -110.821673

https://en.wikipedia.org/wiki/Multiple_independently_targetable_reentry_vehicle

Cylindrical, Time-Encoded Imaging

- A detector is placed in the interior of a cylindrical mask with open and closed elements
- As the mask rotates, the count rate observed by the detector is modulated in time
- Temporal analog to spatial coded aperture

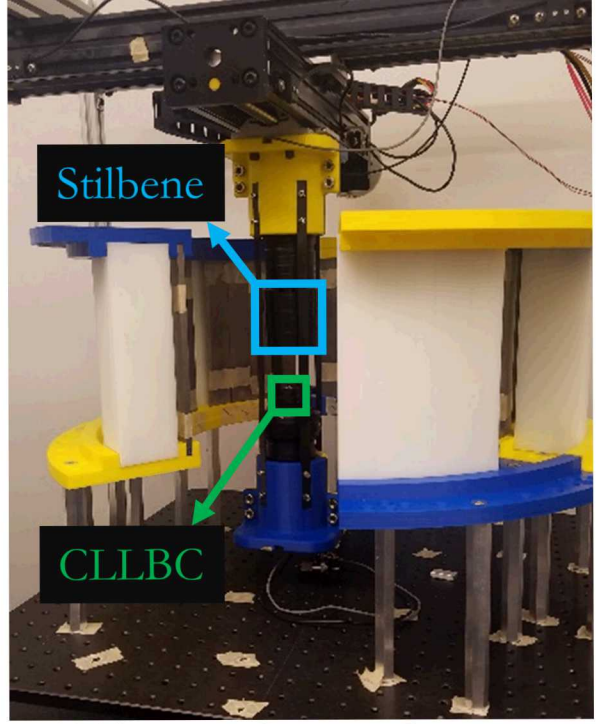

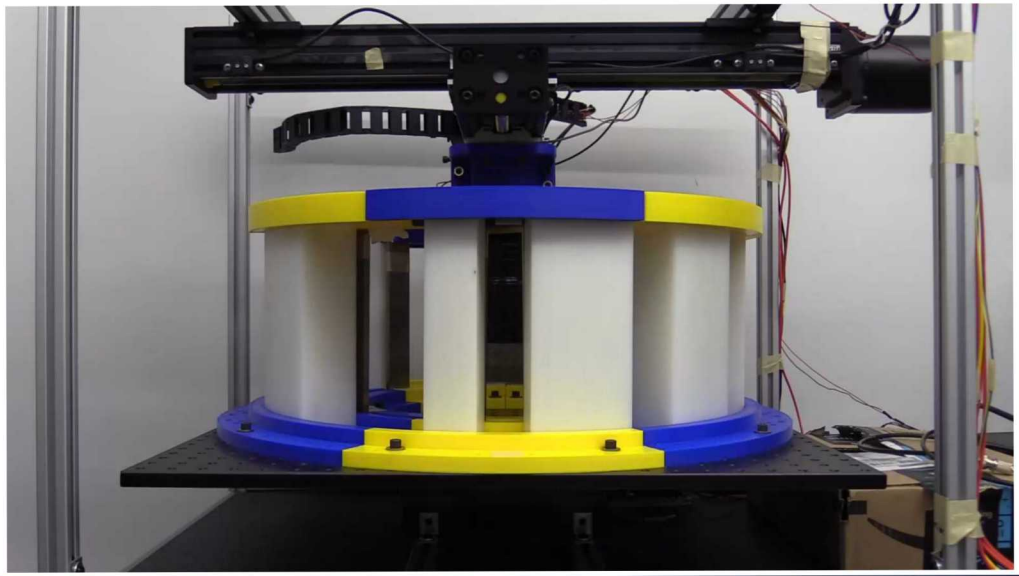

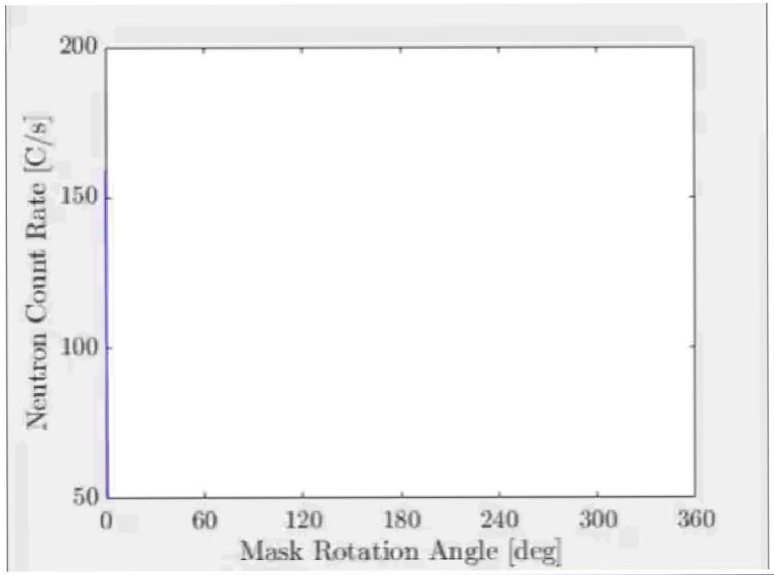

MATADOR System Parameters

Detector	2” Stilbene & 1” CLLBC
Mask Pattern	URA-35
Inner mask radius	17.5 cm
Tungsten thickness	0.635 cm
HDPE thickness	6 cm
Outer mask radius	26 cm

N. P. Shah, J. VanderZanden, and D. K. Wehe, “Design and Construction of a 1-D, Cylindrical, Dual-Particle, Time-Encoded Imaging System,” *Nucl. Inst. Methods Phys. Res. A*, 2019.

Adaptive Imaging

- **Leverage collected data to inform where to collect next set of data**
- Angular resolution is geometry dependent
- Moving the detector changes the angular resolution
- Protocol
  - Conventional: Collect data at center for 100% of allotted time
  - Adaptive: Collect data at center for 10% of total time (initial data) and at "best" position(s) for remaining 90% of allotted time
  - Task: Best angular resolution
    - Proxy: Cramér-Rao lower bound
  - No cost to moving detector

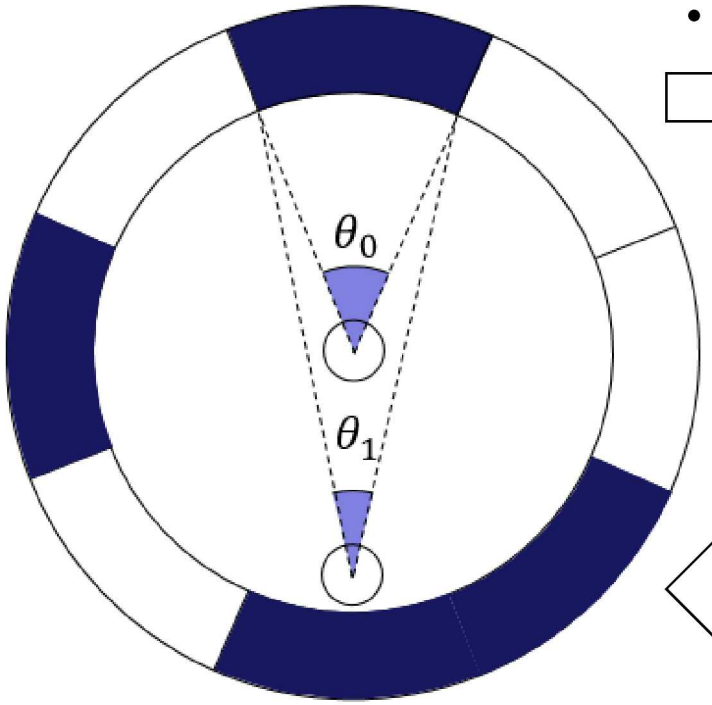

Experimental Data
- Raw digitized pulses

Reconstruction
- MLEM

Update Algorithm
- Task: Best angular resolution

Adaptive Imaging
- Detector position

Proxy for Angular Resolution: Cramér-Rao

- The Cramér Rao lower bound (CRLB) provides a lower bound on the variance of an unbiased estimator
  - **Independent of reconstruction method**, only dependent on the assumed source distribution, background, and system response
- **Intuition: The "sharper" the likelihood function, the easier it is to estimate the parameter(s) of interest**
  - Measures sharpness via curvature (second derivative)
- Find CRLB for all candidate detector positions based on initial data from the center and move to the one with the smallest CRLB value
- Unknown parameters
  - Source strength, source position, background
  - Estimate via maximum likelihood (ML)

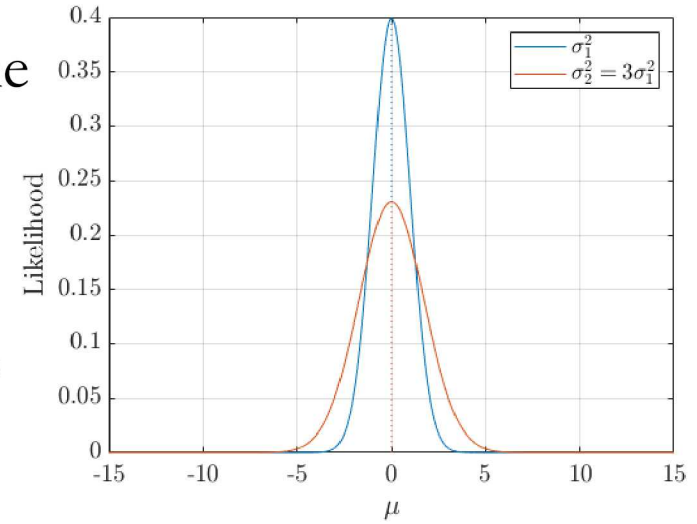

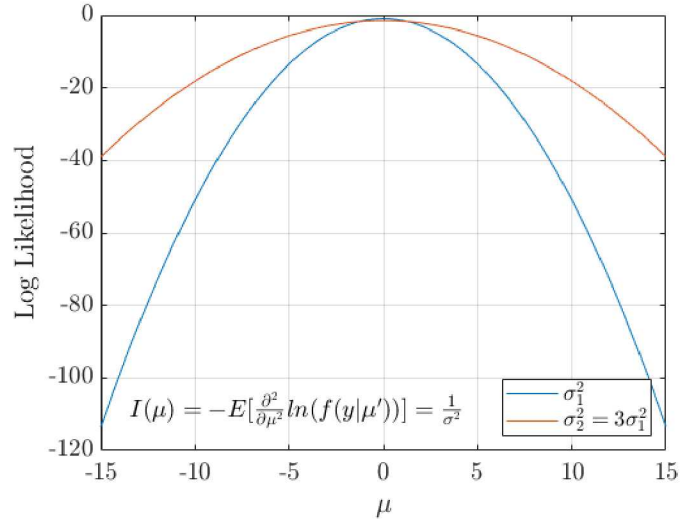

Example: Single Point Source – Initial Scan

- Source: 1.85 mCi Cf-252 at (180°, 90cm)
  - Subsampled to 96.0 μCi
  - Total measurement time: 15 minutes
- Collect **neutron data with 2" Stilbene** at center (10% of total time)
- Estimate unknowns

- Create CRLB map using ML estimates
  - Black points: candidate detector positions
  - Red point: detector position with lowest CRLB
- Move detector and collect next set of data (90% of total time)

Source

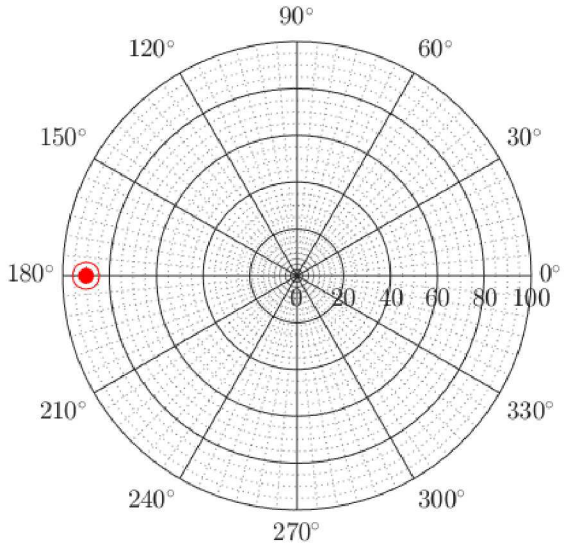

Image from Initial Scan

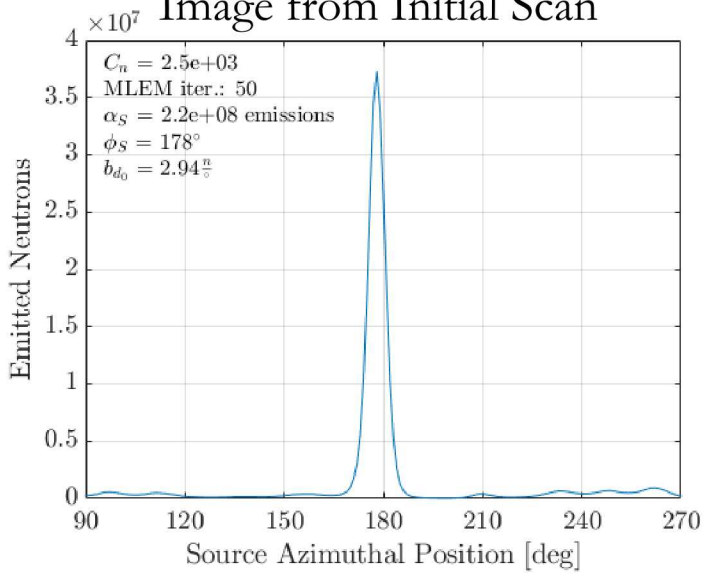

CRLB Map

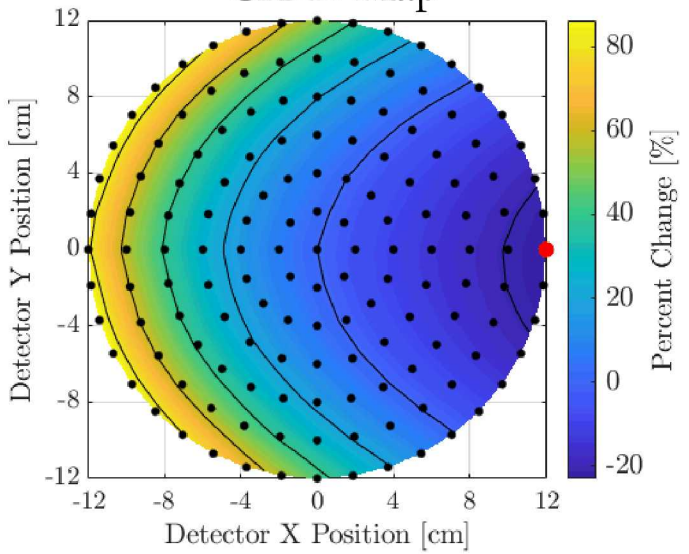

Example: Single Point Source – Comparison

- Conventional: 100% of allotted time with detector at the center
- Adaptive: 10% of allotted time with detector at center and 90% with detector at (12, 0) cm
- Measured counts decrease because of inverse square effects
- **Angular resolution improved ~25%** in line with CRLB predictions

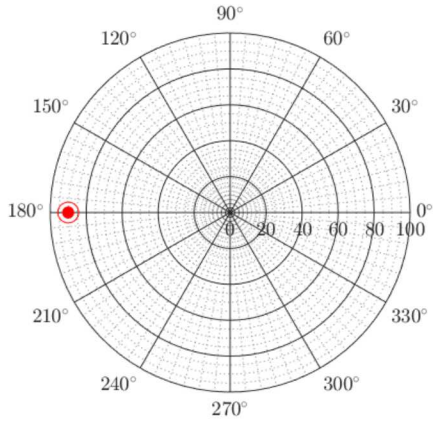

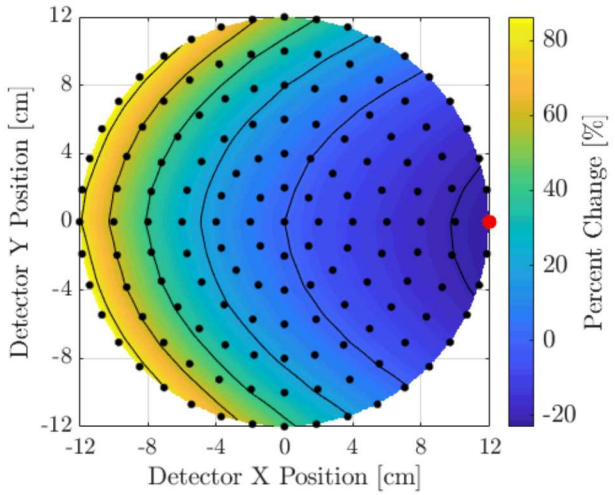

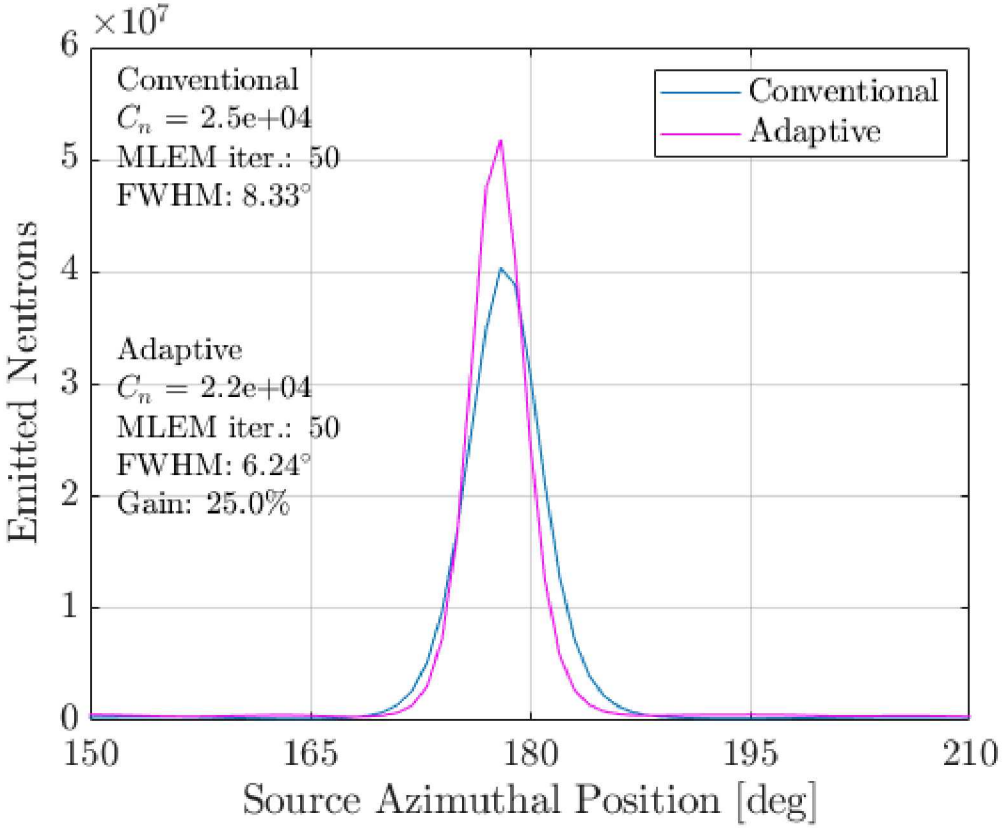

Two Point Sources – Initial Scan

- Source: Two 1.85 mCi Cf-252
  - At (175°, 90cm) & (185°, 90cm)
  - Subsampled to 48.0 μCi each
  - Total measurement time: 15 minutes
- Estimate unknowns from initial scan assuming two sources

- Utility function for combining CRLBs for each source

$$U = \frac{\sqrt{\sigma_{\theta_1}^2 + \sigma_{\theta_2}^2}}{2}$$

Source

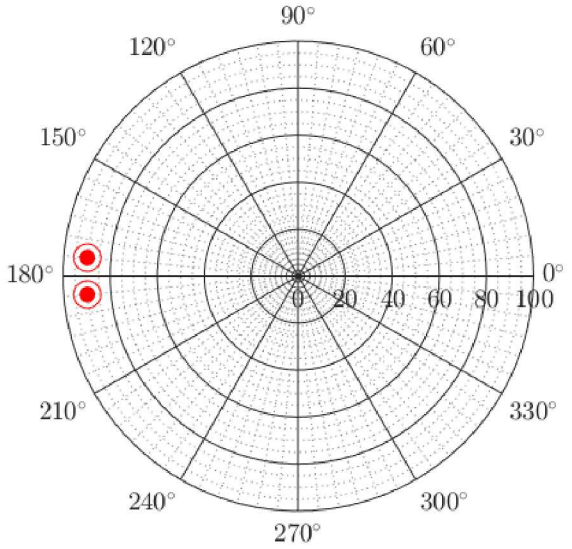

Image from Initial Scan

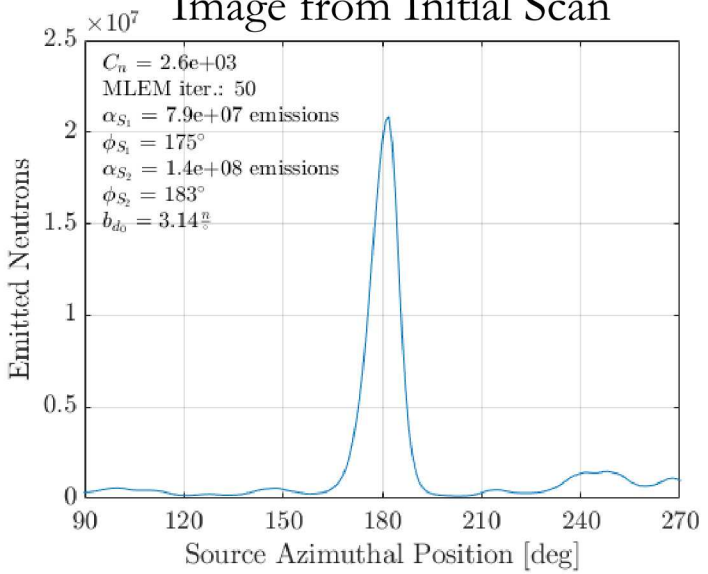

CRLB Map

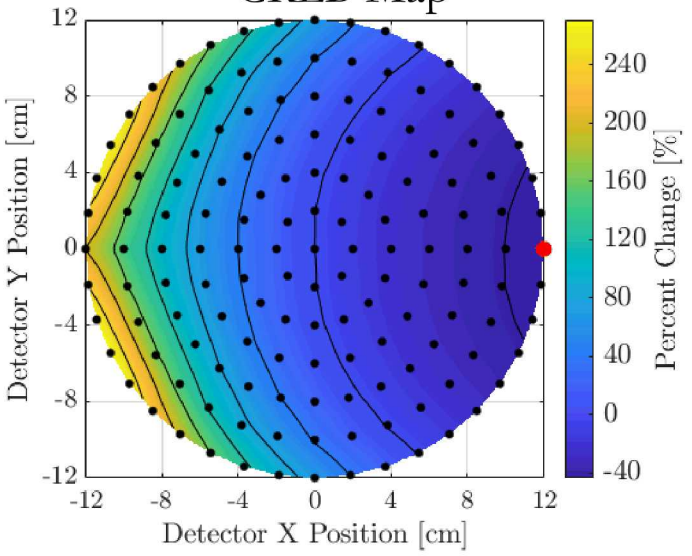

Two Point Sources – Comparison

- After 25,000 neutron counts, the conventional system fails to resolve two equal intensity point sources separated by 10°.
- In the adaptive imaging case, the two sources are clearly resolved.
- Adaptive detector movements lead to better angular resolution.

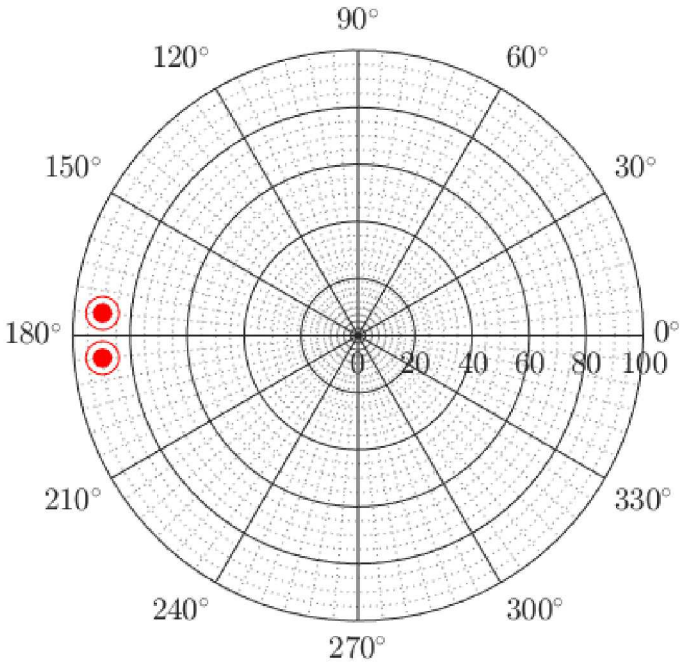

Conventional

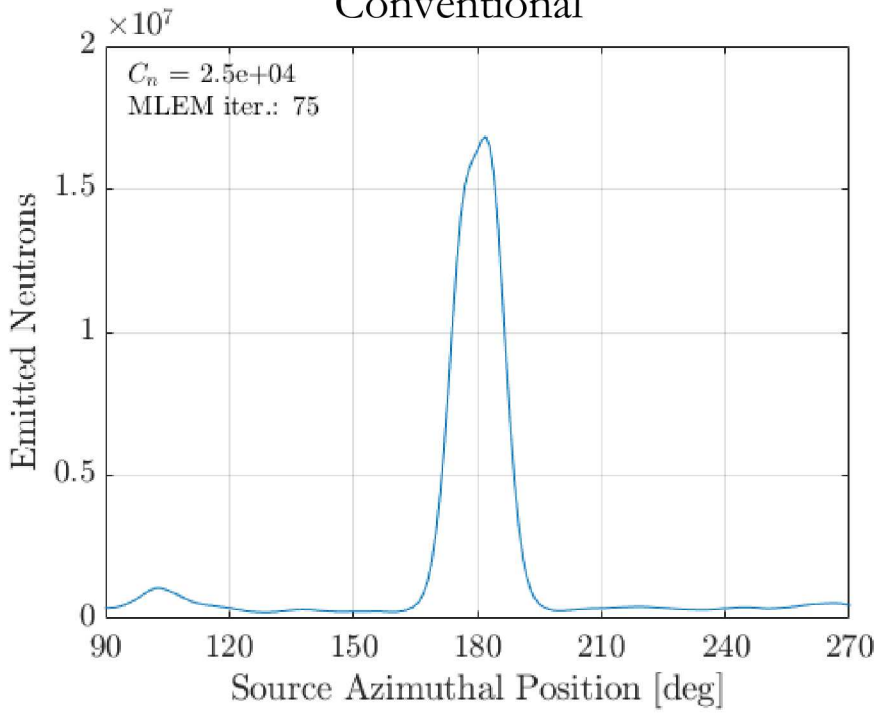

Adaptive

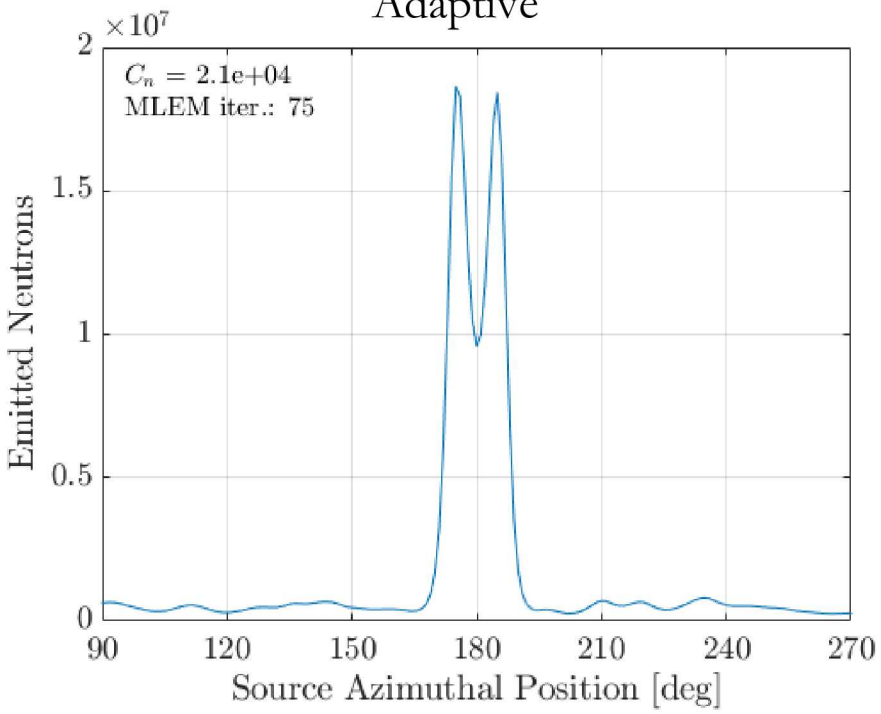

Demonstration using Special Nuclear Material

- Conducted a 4-day measurement campaign at Idaho National Lab in June 2019
- Experiment setup includes 16 high Pu-240 content plates and MOX fuel pins
  - **Complex arrangement of sources**: point sources, two point sources nearby, extended sources, different radial distances, and large activity differences

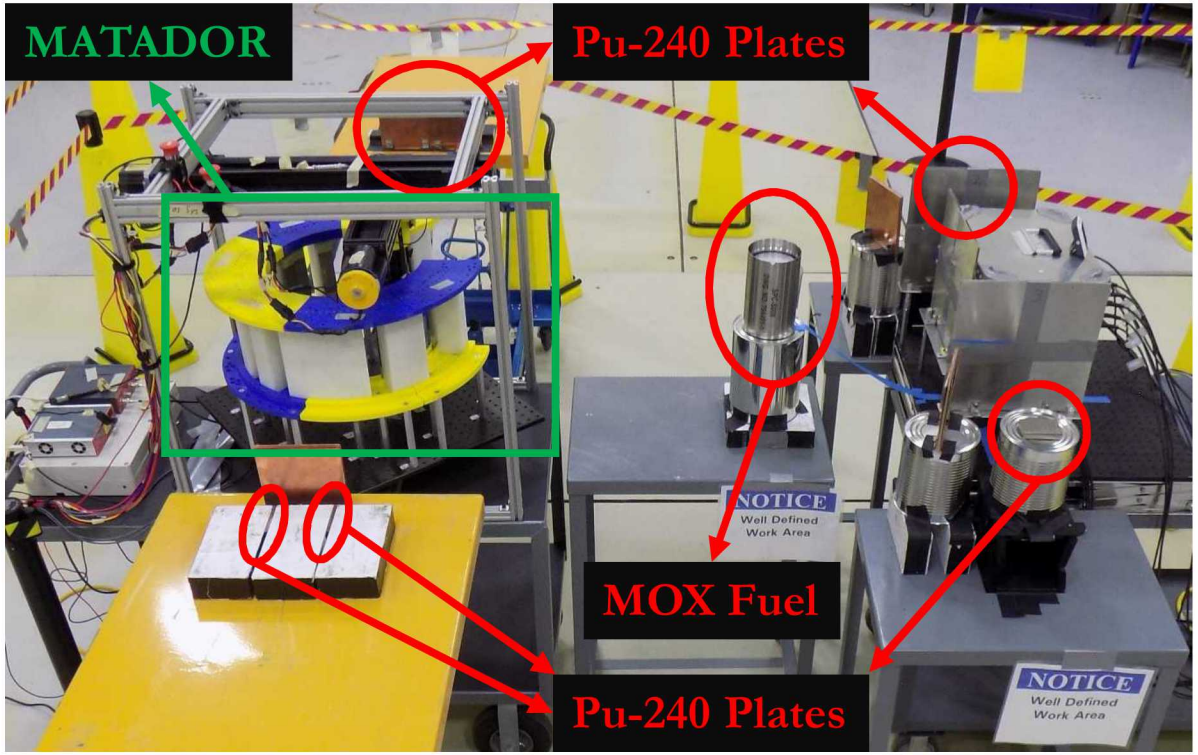

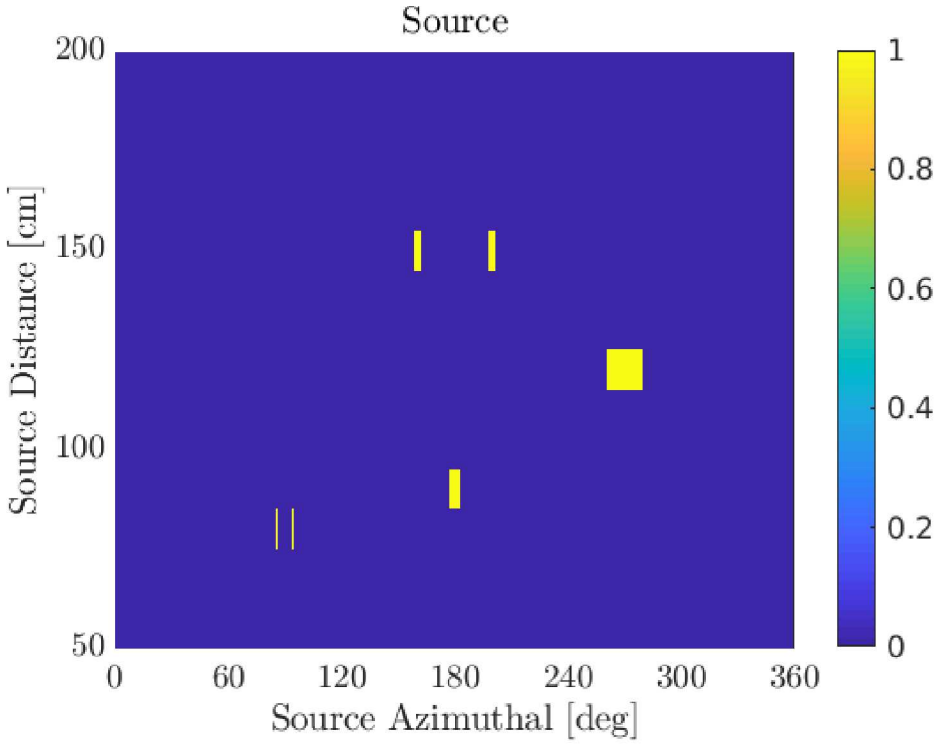

Special thanks to David Chichester, Jay Hix, Scott Thompson, and the entire team at INL that made this measurement possible. Also, special thanks to CVT for funding this measurement campaign.

Demonstration using SNM

- Conventional c-TEI
- **1” CLLBC crystal**
- **250-450 keV gammas**
- T = 36.7 minutes
- MOX source is 10x times hotter than all other sources
- Cannot resolve two point sources
- Cannot estimate radial distance to sources

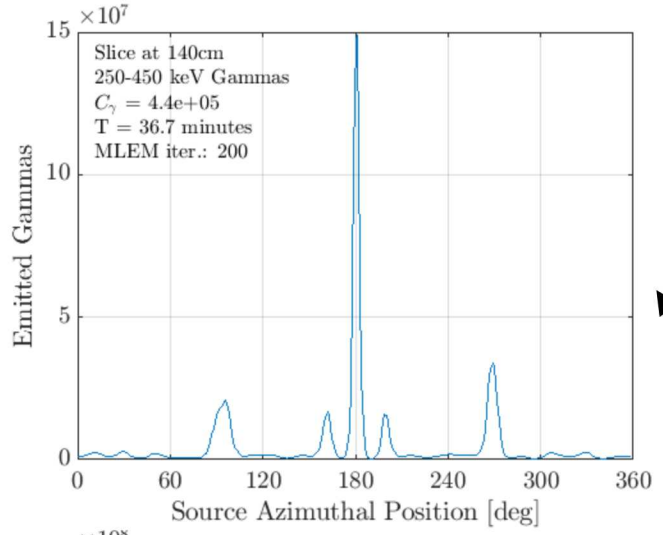

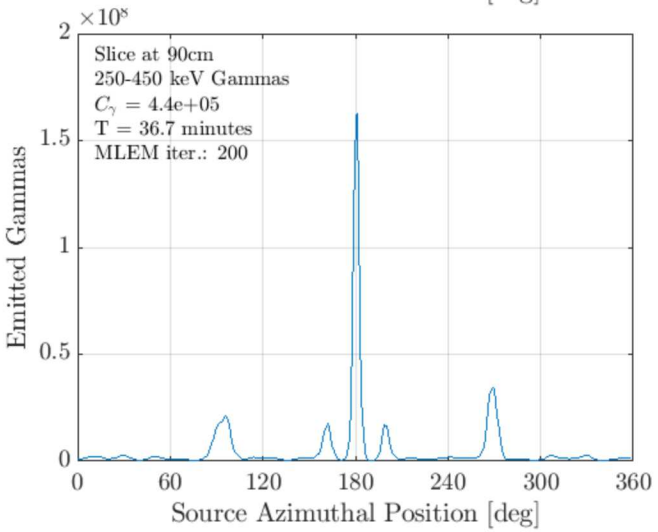

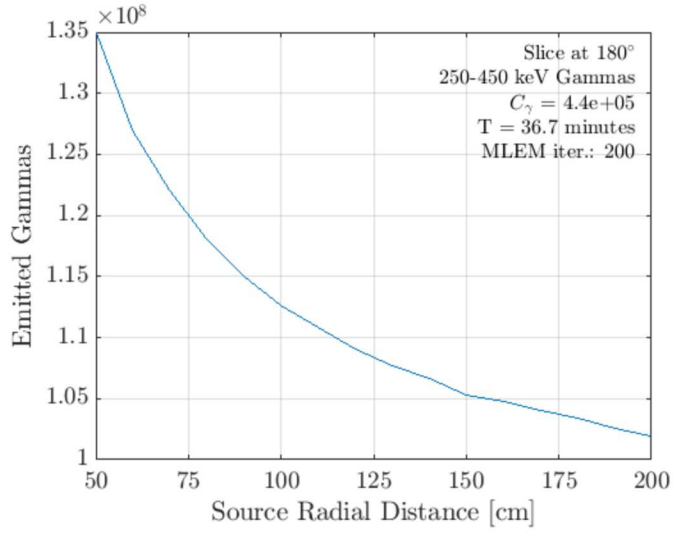

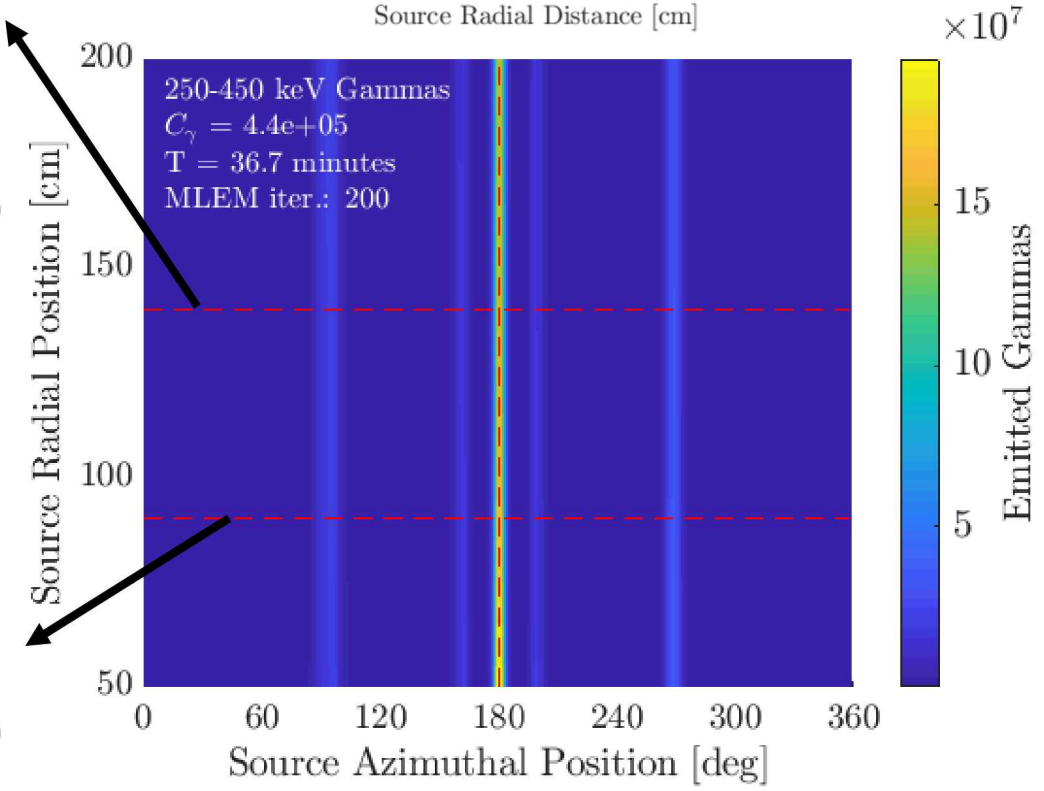

Linear Scale

Demonstration using SNM

- Conventional c-TEI
- 1” CLLBC crystal
- 250-450 keV gammas
- T = 36.7 minutes
- MOX source is 10x times hotter than all other sources
- Cannot resolve two point sources
- Cannot estimate radial distance to sources

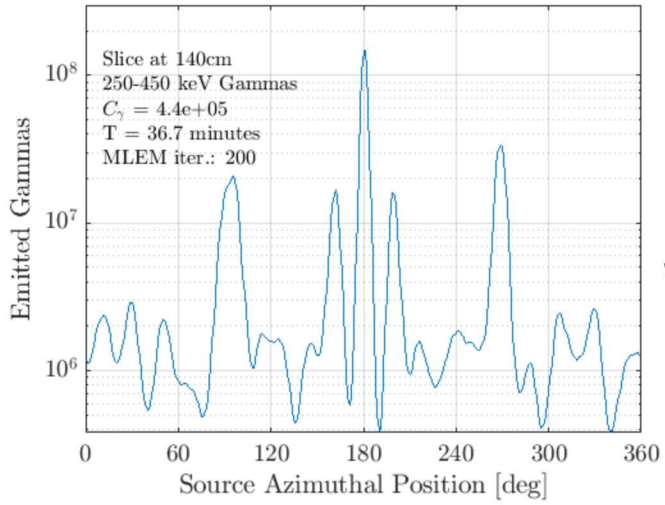

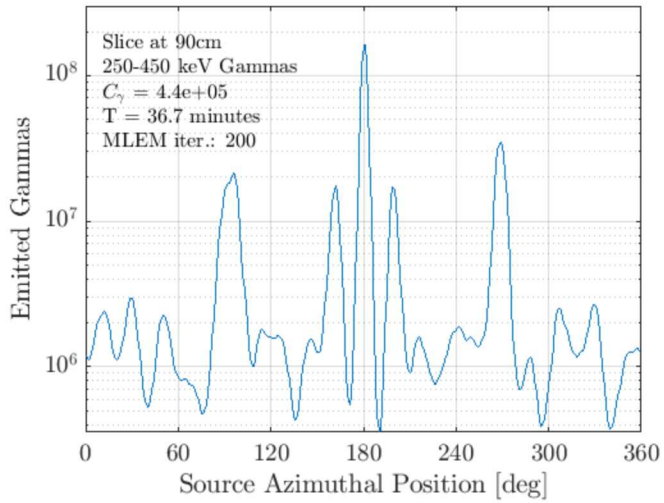

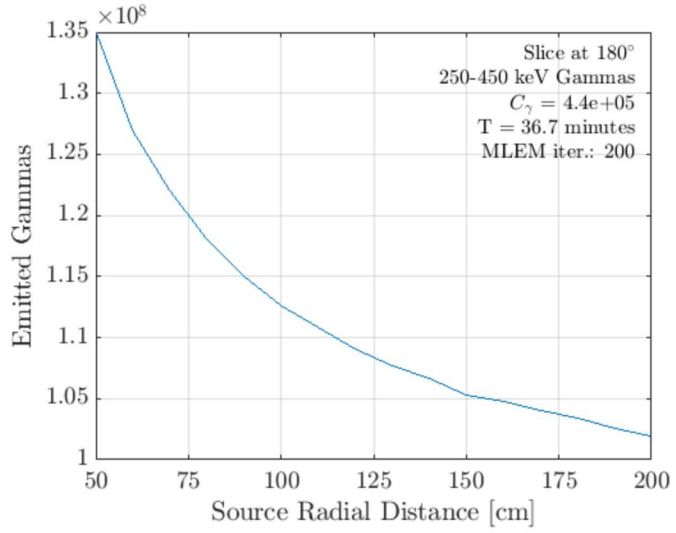

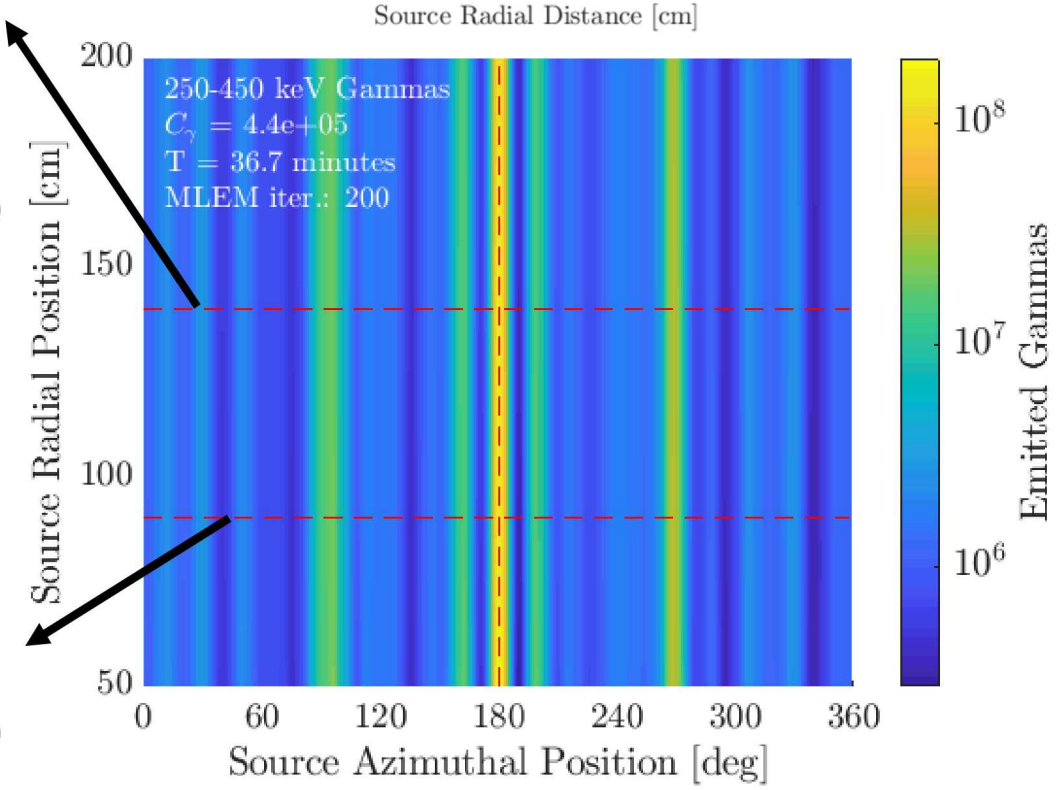

Logarithmic Scale

Demonstration using SNM

- Adaptive c-TEI
- Resolved two point sources
- Ability to provide distance to source estimates
- 22 detector positions (red) were arbitrarily chosen for this reconstruction

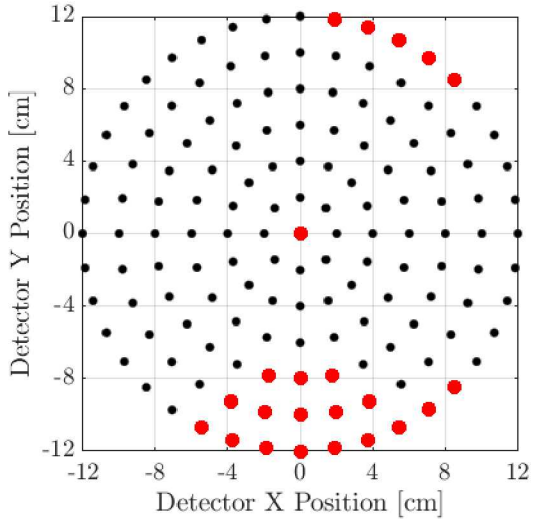

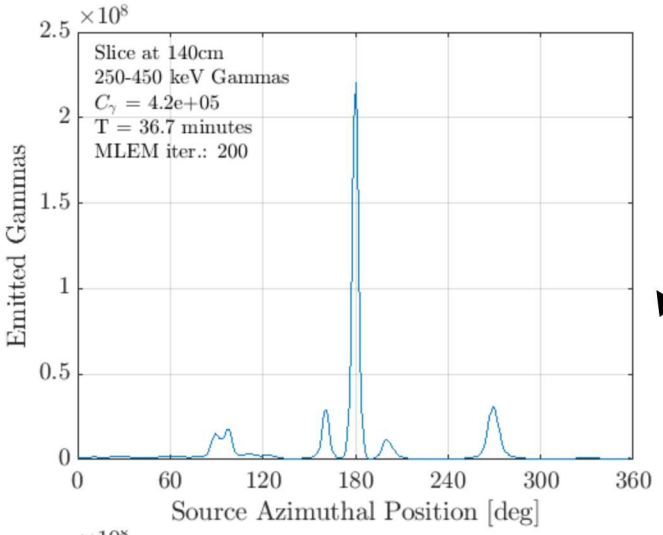

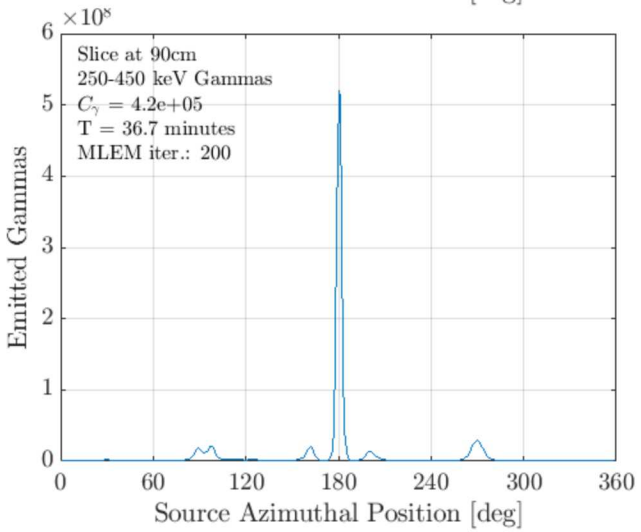

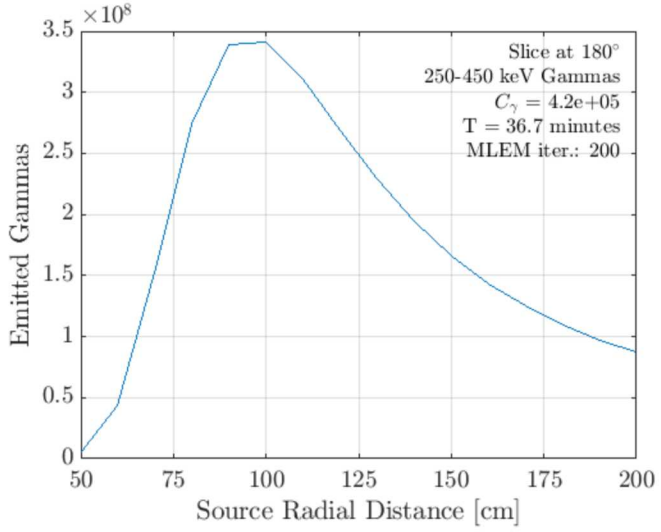

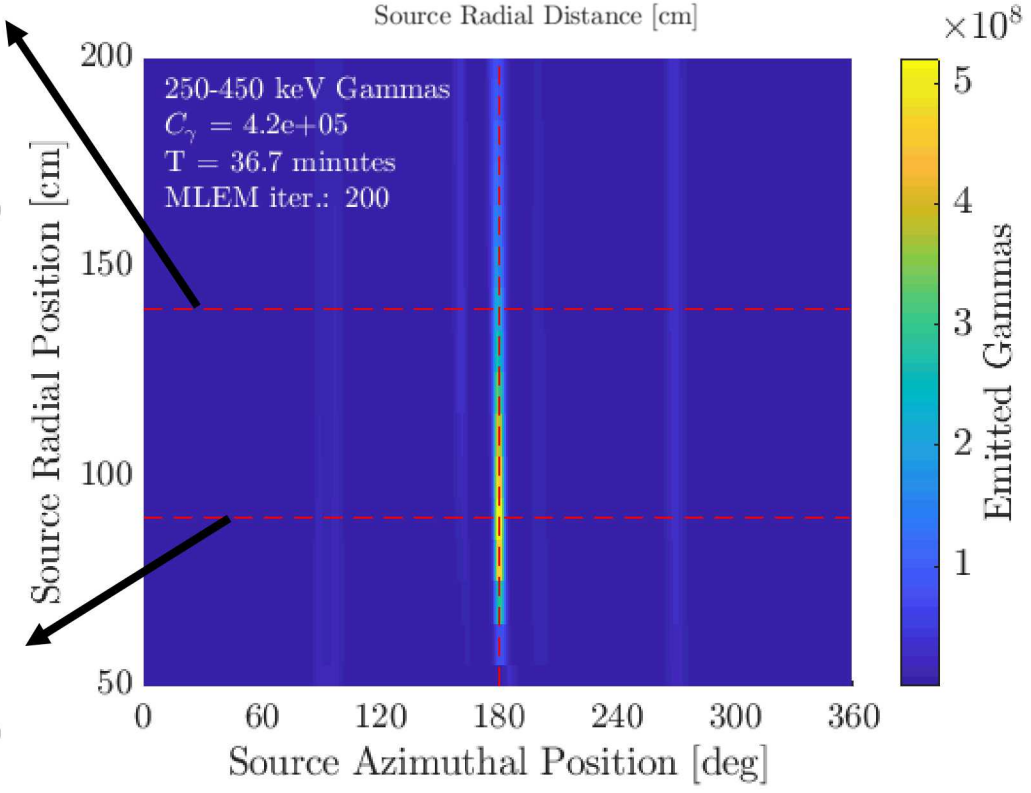

Linear Scale

Demonstration using SNM

- Adaptive c-TEI
- Resolved two point sources
- Ability to provide distance to source estimates
- 22 detector positions (red) were arbitrarily chosen for this reconstruction

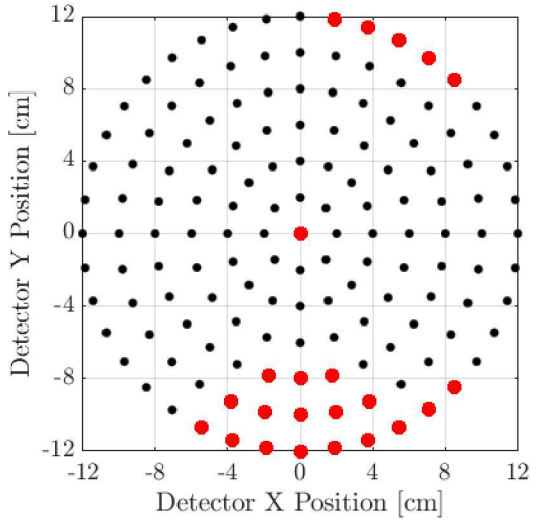

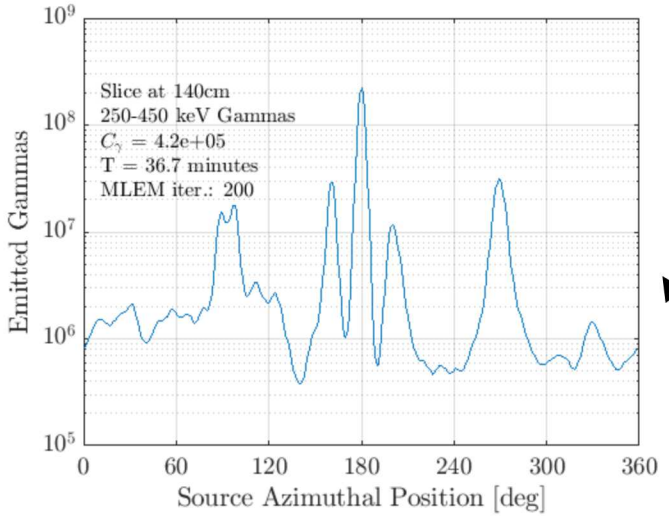

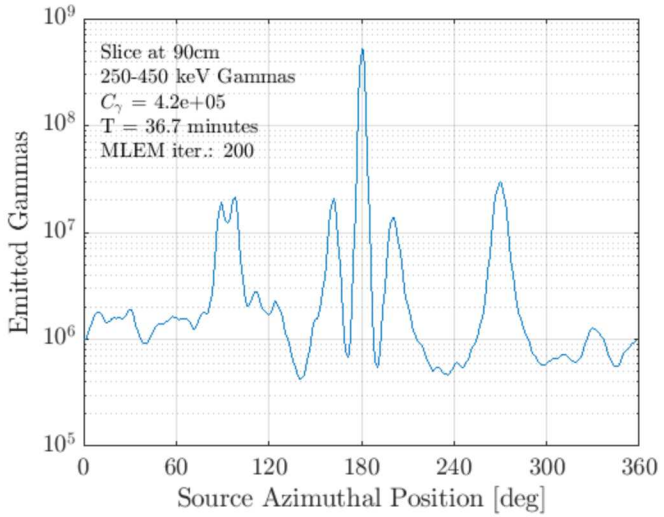

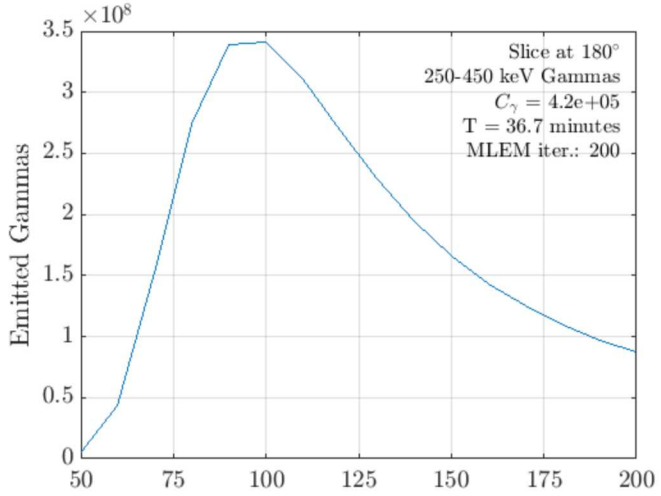

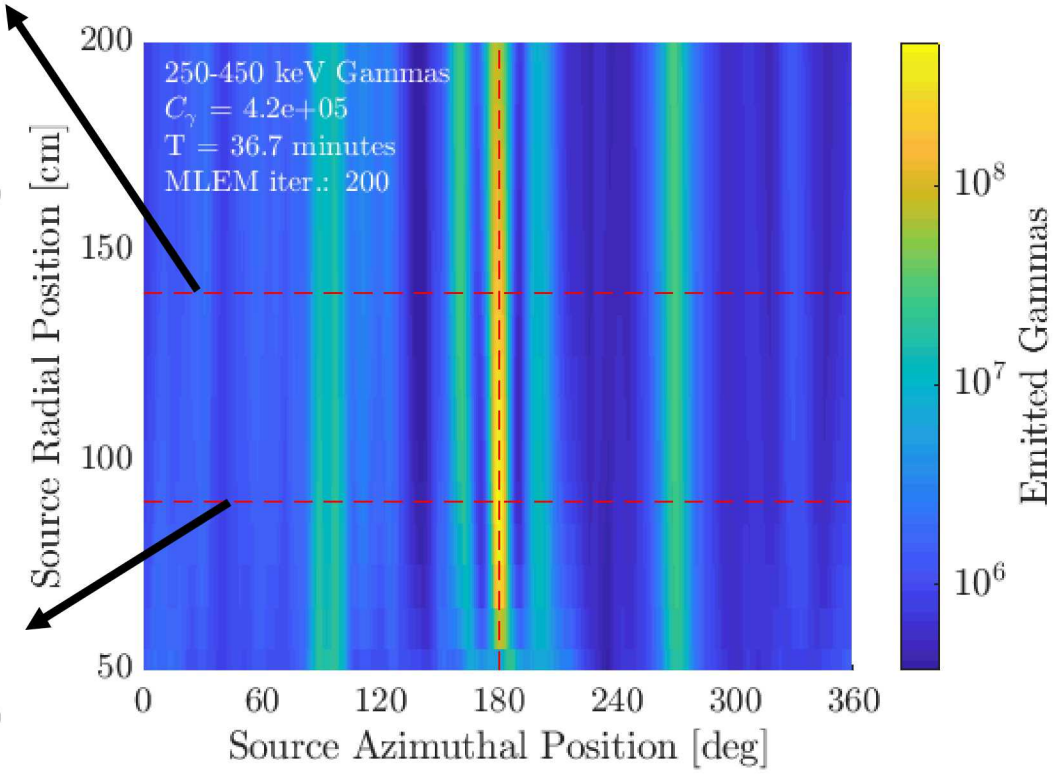

Logarithmic Scale

Comparison

Conventional

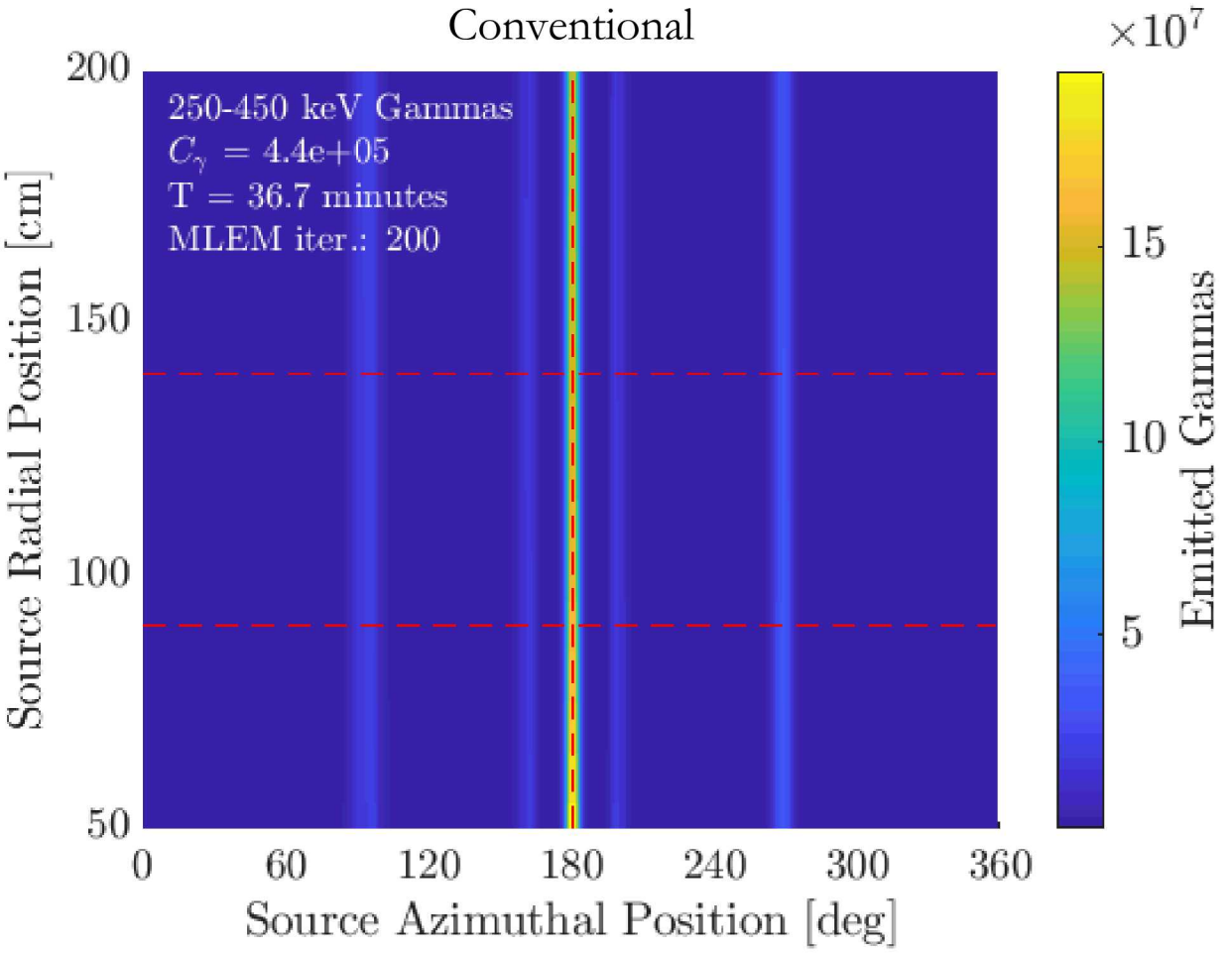

Adaptive

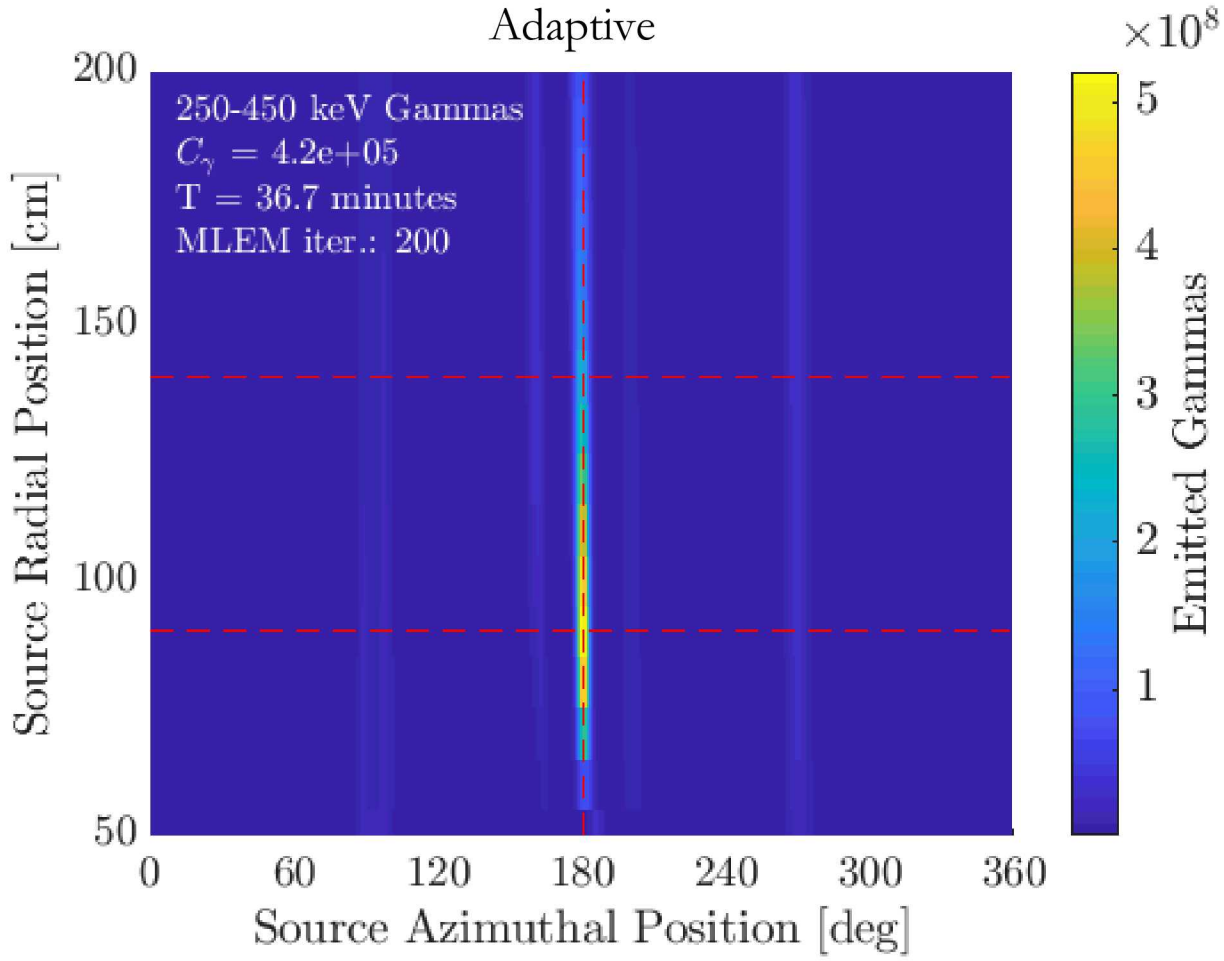

Linear Scale

Comparison

Conventional

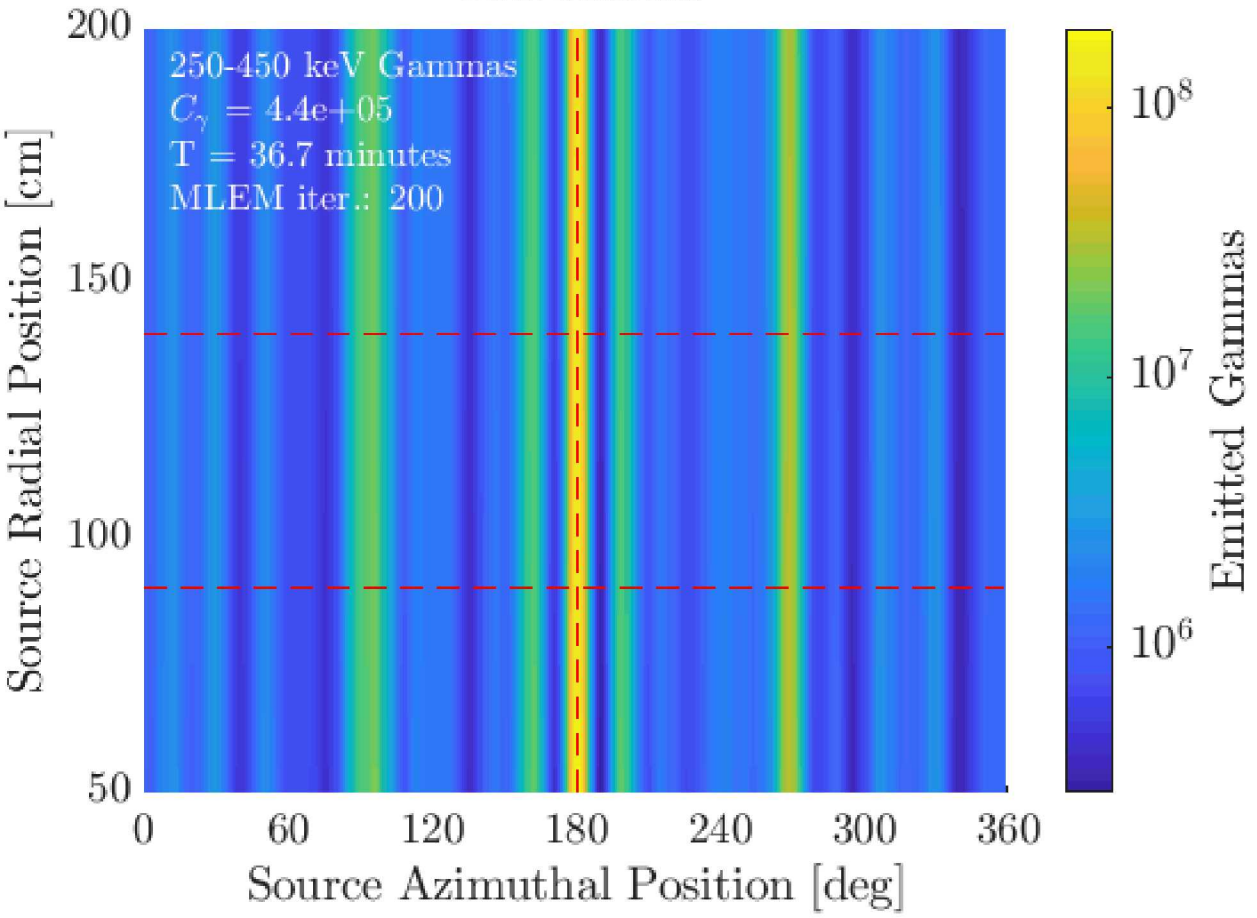

Adaptive

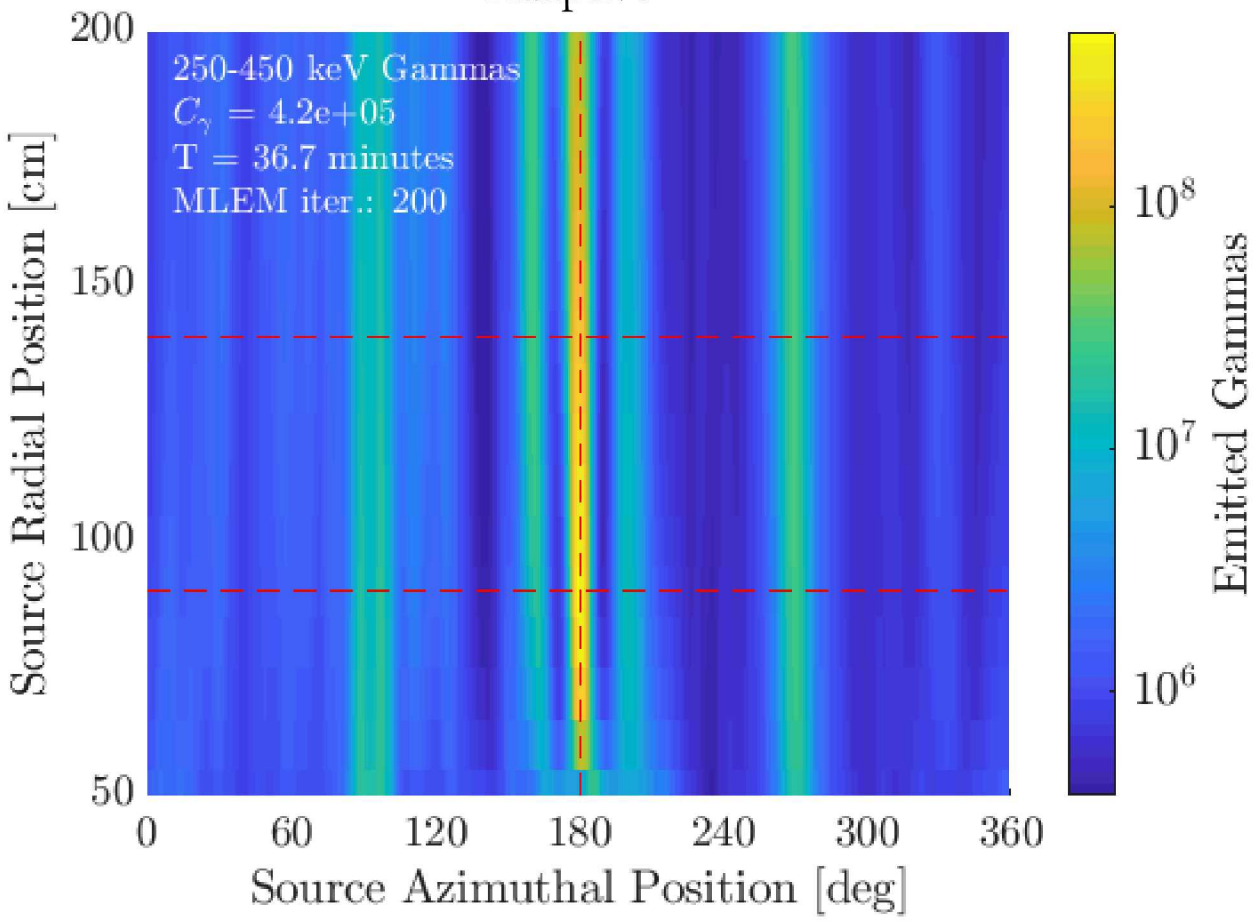

Logarithmic Scale

Conclusions

- Devised an adaptive imaging algorithm to reconstruct higher resolution images
- Laboratory experiments showed improved angular resolution
  - CRLB indicates ~20% gain for point source and ~40% for two point sources
- Demonstrated these benefits by imaging a complex arrangement of SNM at INL

Future Work

- Expand CRLB based algorithm to include multiple point sources and sequential detector movements
- Incorporate optimization for time spent at each detector position

Acknowledgements and Questions?

- This research was performed under appointment to the Nuclear Nonproliferation International Safeguards Fellowship Program sponsored by the National Nuclear Security Administration's Office of International Nuclear Safeguards (NA-241).

- This work was funded in-part by the Consortium for Verification Technology under Department of Energy National Nuclear Security Administration, USA award number DE-NA0002534.

- Special thanks to David Chichester, Jay Hix, Scott Thompson, and the entire team at INL for facilitating the ZPPR measurements.

- Sandia National Laboratories is a multimission laboratory managed and operated by National Technology and Engineering Solutions of Sandia, LLC., a wholly owned subsidiary of Honeywell International, Inc., for the U.S. Department of Energy's National Nuclear Security Administration under contract DE-NA0003525.

- INL release

More on Cramér-Rao Lower Bound

Unknowns: source strength, source position, and background

N_S: Number of sources

N_D: Number of detector positions

$N_{O,d}$: Number of observations at detector position d

$N_O = \sum_{d=1}^{D} N_{O,d}$: Total number of observations

$\boldsymbol{\alpha}$: $N_S \times 1$ vector of source strengths

$\boldsymbol{\phi}$: $N_S \times 1$ vector of source positions

$\boldsymbol{b}$: $N_D \times 1$ vector of backgrounds for each detector position

- Background is treated as constant for all observations at a given detector position

$\boldsymbol{t}$: $N_D \times 1$ vector of measurement times for each detector position

- Measurement time is held constant for all observations at a given detector position

$\boldsymbol{y_d}$: $N_{O,d} \times 1$ vector of observations at detector position d

$$\boldsymbol{y_d} = \left(\sum_{j=1}^{N_S} \alpha[j] A[:, \phi[j]] + \mathbf{1} b[d]\right) t[d]$$

$$\boldsymbol{y} = \left[\boldsymbol{y}_1^T \; \boldsymbol{y}_2^T \ldots \boldsymbol{y}_d^T \ldots \boldsymbol{y}_D^T\right]^T : N_O \times 1 \text{ vector of observations}$$

$$\boldsymbol{\theta} = [\boldsymbol{\alpha}^T \; \boldsymbol{\phi}^T \; \boldsymbol{b}^T]^T$$

$$\ln\left(f(\boldsymbol{y}|\boldsymbol{\theta}')\right) = \sum_{i=1}^{N_O} y_i \ln(\overline{y_i}) - \overline{y_i} - \ln(y_i!)$$

$$I(\boldsymbol{\theta}) = -E\left[\frac{\partial^2}{\partial \boldsymbol{\theta} \partial \boldsymbol{\theta}^T} \ln\left(f(\boldsymbol{y}|\boldsymbol{\theta}')\right)\right]$$

$$I(\boldsymbol{\theta}) = \sum_{i=1}^{N_O} \frac{(\nabla_{\boldsymbol{\theta}} \overline{y_i})(\nabla_{\boldsymbol{\theta}^T} \overline{y_i})}{\overline{y_i}}$$

$$\frac{\partial \overline{y_i}}{\partial \alpha_j} = A[i, \phi[j]] t[d];$$

$$\frac{\partial \overline{y_i}}{\partial \phi_j} = \alpha_j t[d] \frac{\partial A[i,\phi[j]]}{\partial \phi_j};$$

$$\frac{\partial \overline{y_i}}{\partial b_d} = t[d]$$

$$\frac{\partial A[i,\phi[j]]}{\partial \phi_j} = \frac{A[i,\phi_j + \Delta\phi] - A[i,\phi_j - \Delta\phi]}{2\Delta\phi}$$

$$Cov_{\boldsymbol{\theta}}(\hat{\boldsymbol{\theta}}) \geq I(\boldsymbol{\theta})^{-1}$$

Theoretical Basis – Alternative Explanation

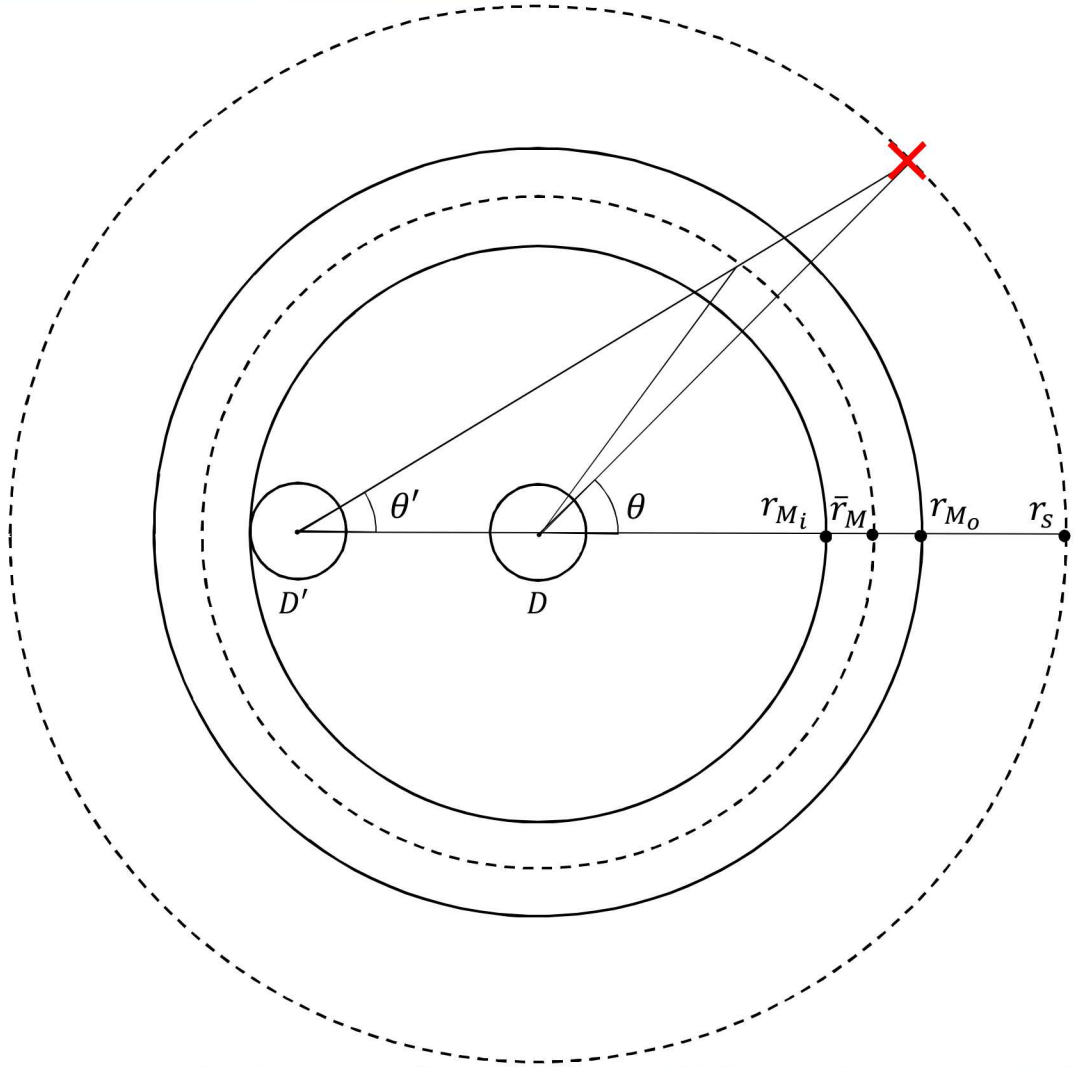

- Imagine particles streaming in a straight line from the source to the detector in the center
- As the detector moves off center, the angular position at which the source particles are intersecting the mask moves
- If there were two sources mirrored, then they would move further apart in the mask space.
- This leads to better resolution.

With Source Radius

- Resolution advantage from offsetting decreases as the source radius decreases
- Detector is offset to 11.25 cm

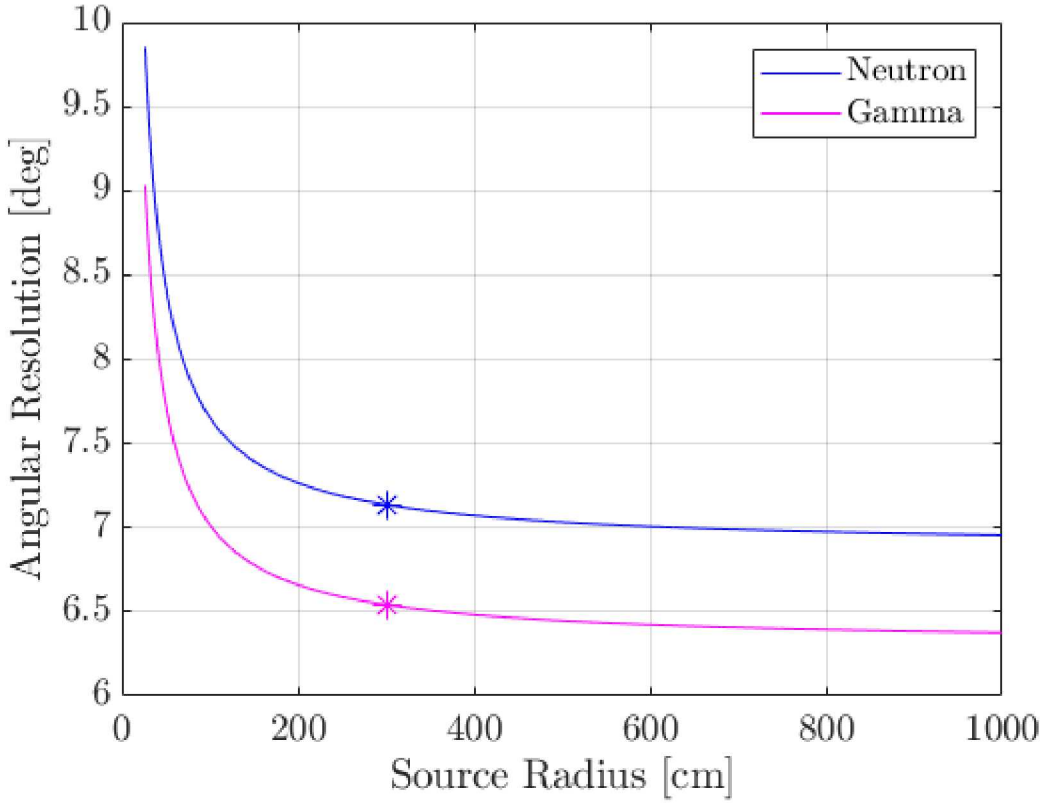

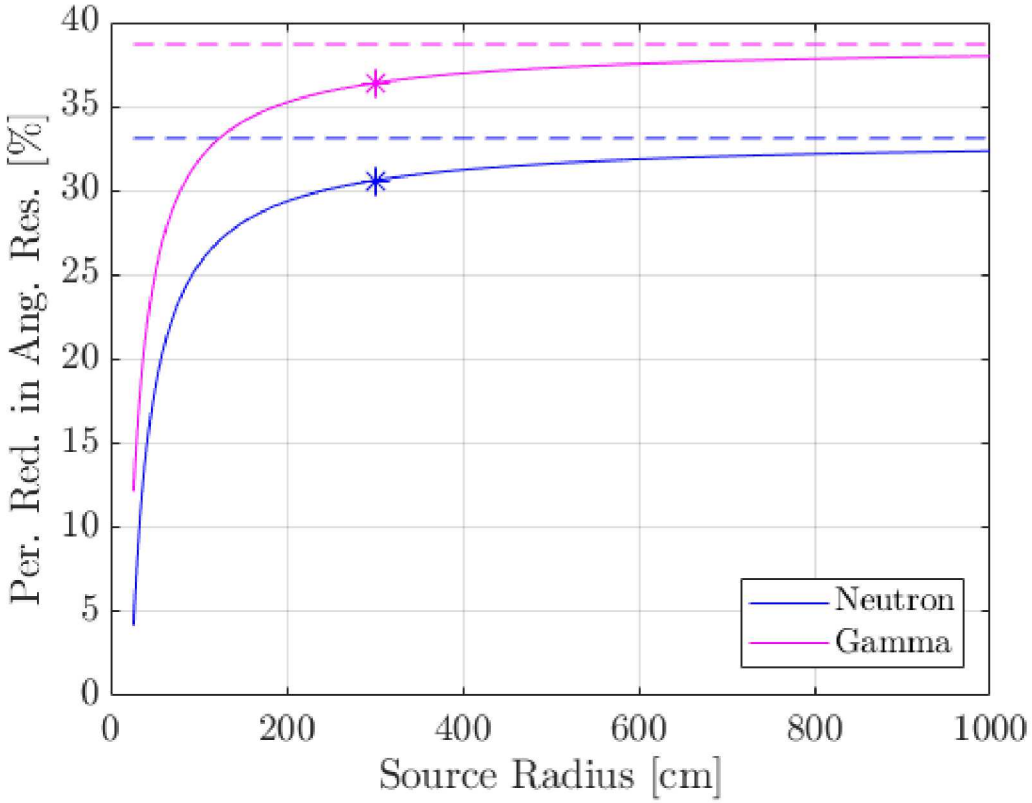

Experimental Data

C. Sosa, "The Importance of Light Collection Efficiency in Radiation Detection Systems That Use Organic Scintillators", UM Thesis, 2018.

- Stilbene is a organic scintillator
  - Coupled to photomultiplier tube (R6231-100-001)
  - Sensitive to gamma rays and fast neutrons
  - Pulse shape discrimination to separate the two
- DT5730, 2 ns sampling, 14 bit digitizer
- DT5533 0-1500 (neg) high voltage supply

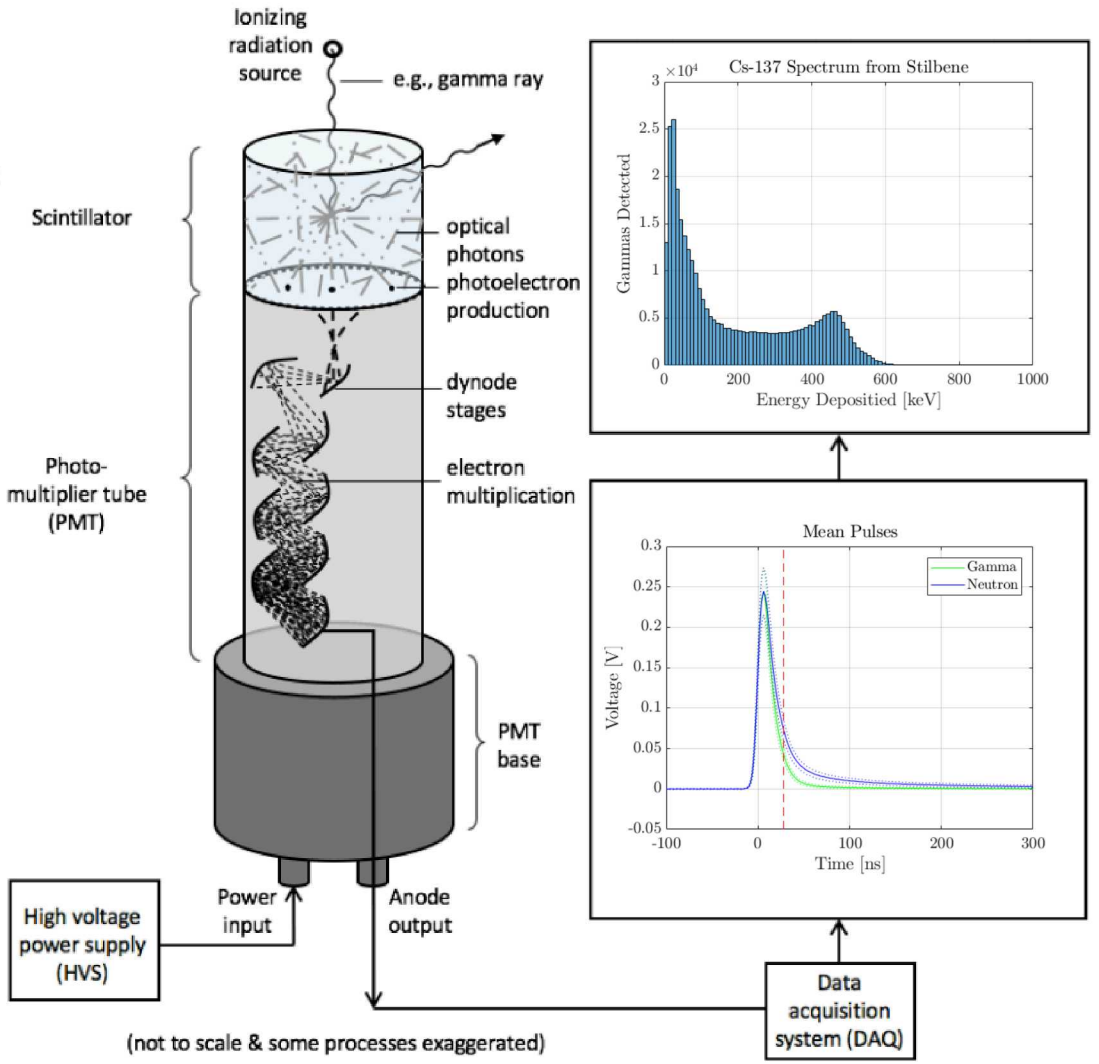

Bayesian PSD

- Replication of work by M. Monterial
- PSD via charge integration method
- Used Cf-252 data to find marginal probability distributions

$$P_{E_i}(n|s) = \frac{f_{n,E_i}(s)}{f_{\gamma,E_i}(s)R_{\gamma/n,E_i} + f_{n,E_i}(s)} \qquad f_{E_i}(s) = \frac{1}{\sigma_{E_i}\sqrt{2\pi}} e^{-\frac{(s-\mu_{E_i})^2}{2\sigma_{E_i}^2}}$$

$$P_{E_i}(\gamma|s) = \frac{f_{\gamma,E_i}(s)R_{\gamma/n,E_i}}{f_{\gamma,E_i}(s)R_{\gamma/n,E_i} + f_{n,E_i}(s)}$$

$$R_{\gamma/n,E_i}(E) = \frac{N_{\gamma,E_i}}{N_{n,E_i}}$$

$$N_{\gamma,E_i} = \sum_{s\in E_i} P(\gamma|s) \quad N_{n,E_i} = \sum_{s\in E_i} P(n|s)$$

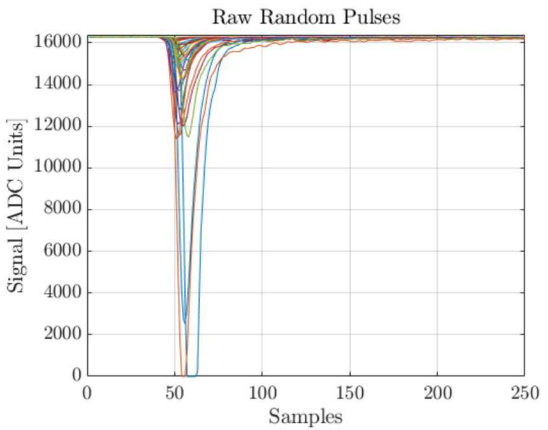

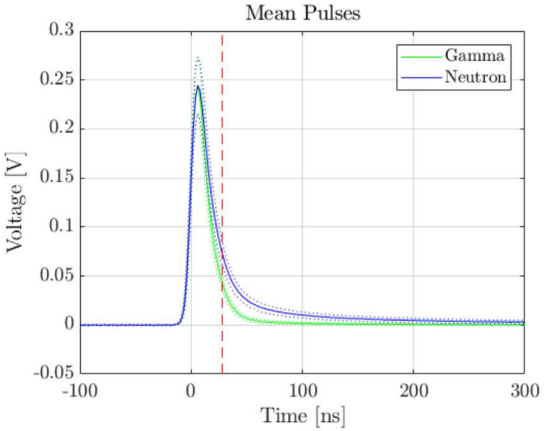

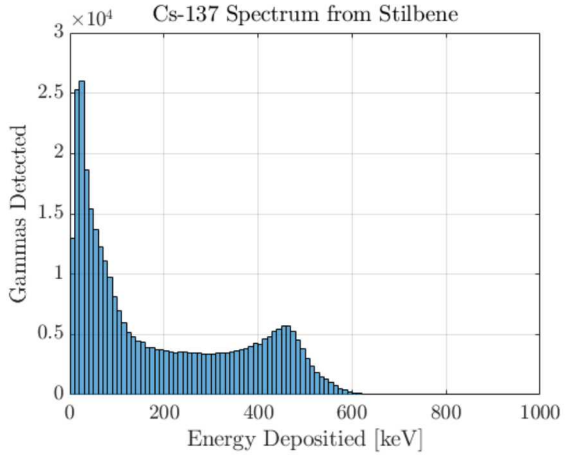

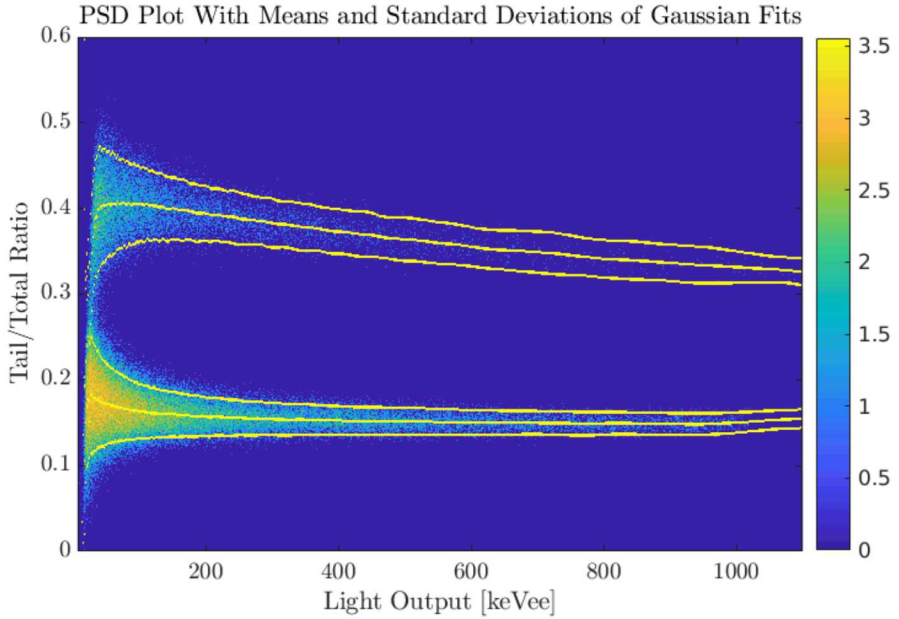

M. Monterial, "Application of Bayes' theorem for pulse shape discrimination", NIMA, 2015.

Thanks to Konrad Rauscher for implementing this Bayesian PSD algorithm

Large and offset detector model (c-TEI)

- Solution: break apart the mask and detector into smaller elements and find the response for each
  - Mask slices are thin such that they are planes
  - Detector response found via simulations
  - As a function of energy, particle, and mask material
- Modified ray tracing (no mask rotation necessary)

$$\boldsymbol{o} = \mathrm{A}\boldsymbol{s};\ \mathrm{A}[:,\mathrm{j}] = \sum_{i=0}^{N_d-1} D[i]e^{-\lambda_M \boldsymbol{t}'_M}\boldsymbol{\tau}$$

$$\boldsymbol{t}'_M\left(\theta_m\left(\vec{r}_{D_i},\vec{r}_{S_j}\right)\right) = \sum_{m=0}^{N_m-1}\frac{t_m \boldsymbol{a}\left[\theta_m\left(\vec{r}_{D_i},\vec{r}_{S_j}\right)\right]}{\cos\left(\theta_m\left(\vec{r}_{D_i},\vec{r}_{S_j}\right)\right)}$$

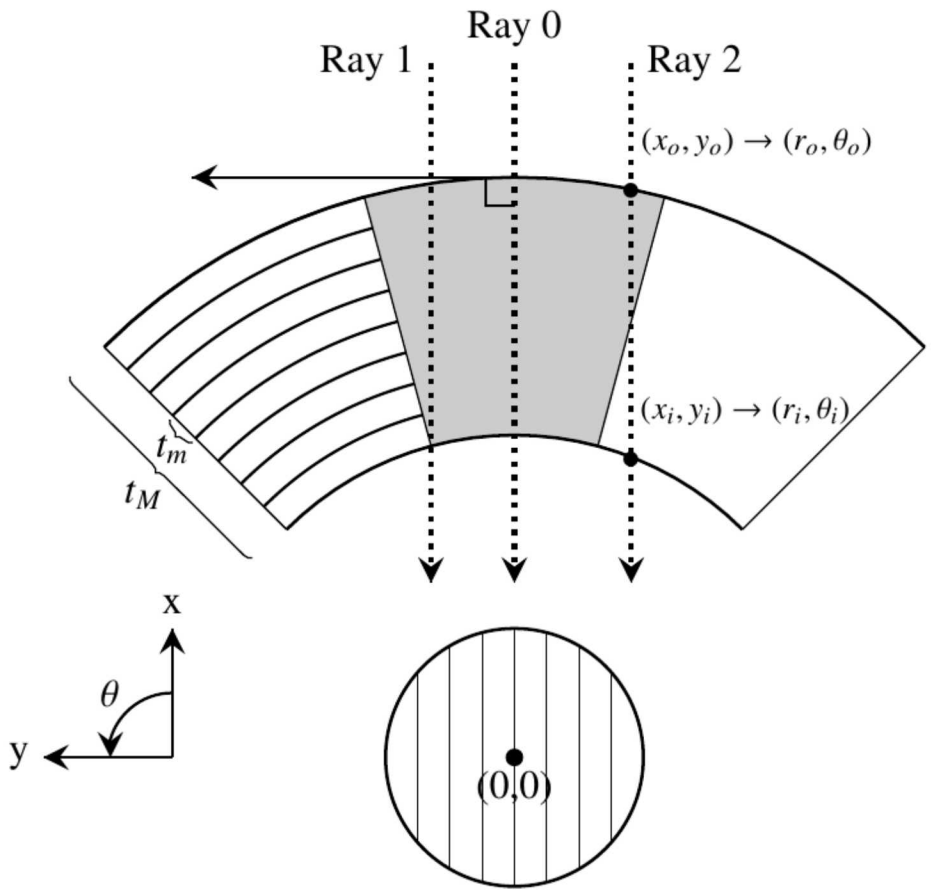

Position Dependent Angular Resolution (Offset)

- PSF is shift variant
- Detector-to-mask distance changes with source position
- Thick mask elements distort open elements

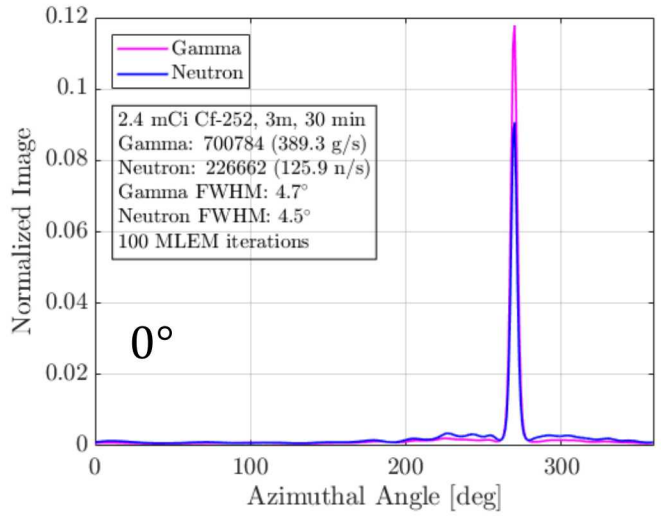

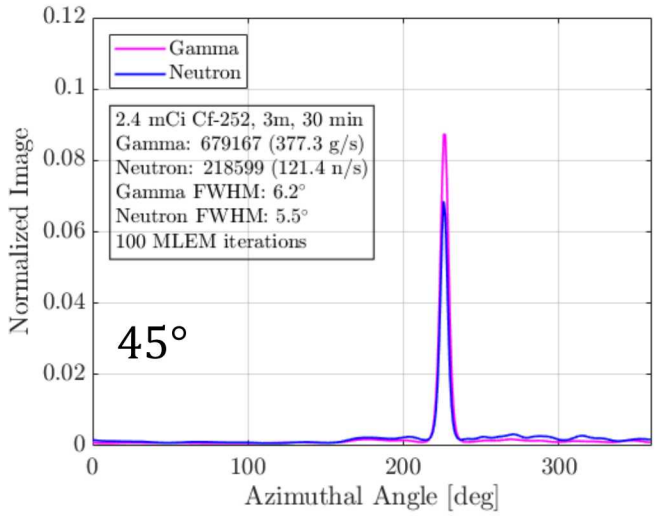

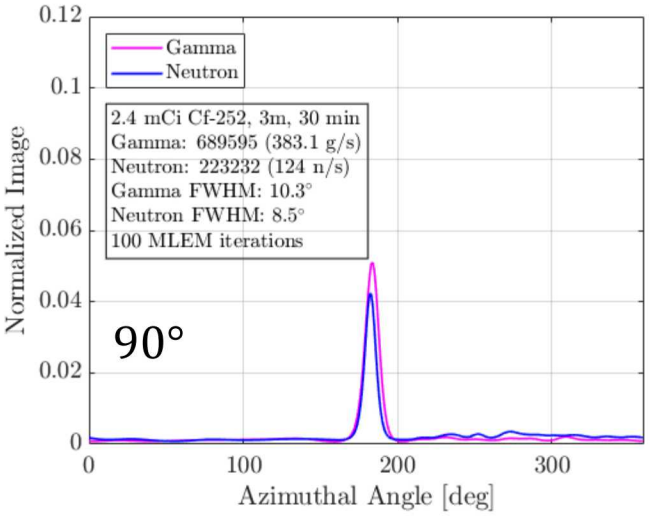

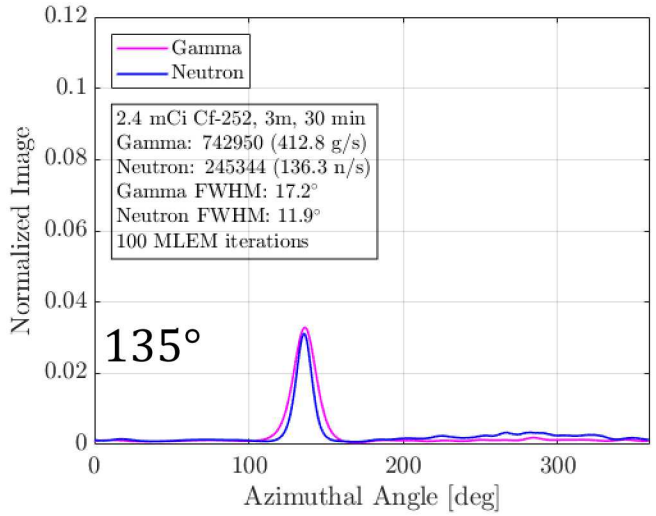

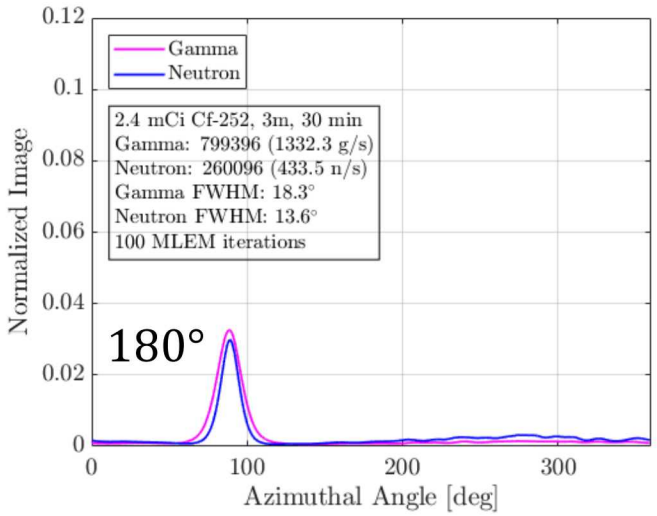

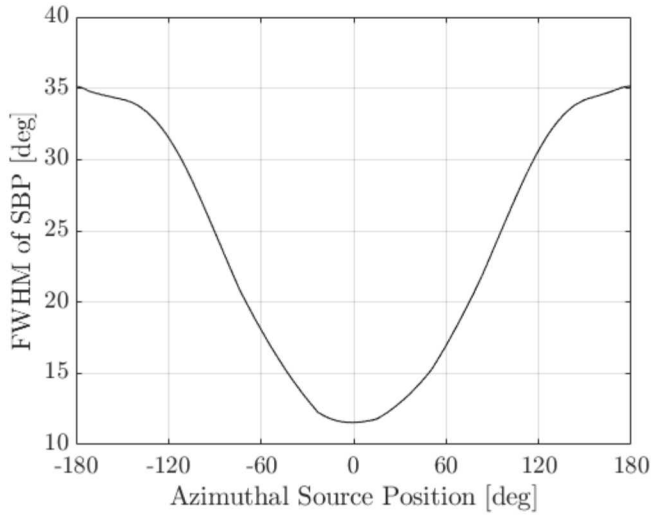

Tailoring the System Response

- Conventional: $y = Ax; A\ is\ I_c \times J_c$. Typically for MATADOR, $I_c = 360$ and $J_c = 360$
- Adaptive: $y = Ax; A\ is\ I_a \times J_a$. Adaptive: $I_a = ??$ and $J_a = J_c = 360$
- What row (or block) should we add to our system response matrix to accomplish … ?

$$\hat{A}^{+1} = \underset{A^{+1}(D,M,\tau)\in\mathbb{A}}{\operatorname{argmin}} \mathbf{E}(\psi(y, A^k, A^{+1}, \hat{x})) \qquad \hat{x} \Rightarrow SBP, FBP, MLEM, Other$$

$$A^{k+1} = [A^k; \hat{A}^{+1}]$$

- $\psi(y, A^k, A^{+1}, \hat{x})$ is application specific
  - Tractable
  - Constrain $\mathbb{A}$ vs include cost of moving to A^{+1}

$$\psi(y, A^k, A^{+1}, \hat{x}) = \text{Task}(y, A^k, A^{+1}, \hat{x}) + \beta Cost(A^k, A^{+1})$$

- Algorithm? Brute force? …

$$\mathbb{A} = \begin{matrix}\text{Pick blocks}\\ \left\{\right.\end{matrix}\begin{bmatrix} \begin{bmatrix} A_{D_1,M_1,1} & \cdots & A_{D_1,M_1,J} \\ \vdots & \ddots & \vdots \\ A_{D_1,M_{end},1} & \cdots & A_{D_1,M_{end},J} \end{bmatrix} \\ \begin{bmatrix} A_{D_2,M_1,1} & \cdots & A_{D_2,M_1,J} \\ \vdots & \ddots & \vdots \\ A_{D_2,M_{end},1} & \cdots & A_{D_2,M_{end},J} \end{bmatrix} \\ \vdots \\ \begin{bmatrix} A_{D_i,M_1,1} & \cdots & A_{D_i,M_1,J} \\ \vdots & \ddots & \vdots \\ A_{D_i,M_{end},1} & \cdots & A_{D_i,M_{end},J} \end{bmatrix} \\ \vdots \\ \begin{bmatrix} A_{D_{end},M_1,1} & \cdots & A_{D_{end},M_1,J} \\ \vdots & \ddots & \vdots \\ A_{D_{end},M_{end},1} & \cdots & A_{D_{end},M_{end},J} \end{bmatrix} \end{bmatrix}\begin{matrix}\leftarrow\\ \leftarrow\\ \leftarrow\\ \\ \leftarrow\\ \\ \leftarrow\\ \\ \\ \end{matrix}$$

Pick rows